

AWARD NUMBER: W81XWH-17-1-0134

TITLE: Interrogating the Mechanism of Long Noncoding RNA ARlnc-1 in Regulating AR Signaling

PRINCIPAL INVESTIGATOR: Yajia Zhang

CONTRACTING ORGANIZATION: University of Michigan
Ann Arbor, MI 48109-2800

REPORT DATE: AUGUST 2019

TYPE OF REPORT: Final Report

PREPARED FOR: U.S. Army Medical Research and Materiel Command
Fort Detrick, Maryland 21702-5012

DISTRIBUTION STATEMENT: Approved for Public Release;
Distribution Unlimited

The views, opinions and/or findings contained in this report are those of the author(s) and should not be construed as an official Department of the Army position, policy or decision unless so designated by other documentation.

REPORT DOCUMENTATION PAGE

Form Approved
OMB No. 0704-0188

Public reporting burden for this collection of information is estimated to average 1 hour per response, including the time for reviewing instructions, searching existing data sources, gathering and maintaining the data needed, and completing and reviewing this collection of information. Send comments regarding this burden estimate or any other aspect of this collection of information, including suggestions for reducing this burden to Department of Defense, Washington Headquarters Services, Directorate for Information Operations and Reports (0704-0188), 1215 Jefferson Davis Highway, Suite 1204, Arlington, VA 22202-4302. Respondents should be aware that notwithstanding any other provision of law, no person shall be subject to any penalty for failing to comply with a collection of information if it does not display a currently valid OMB control number. **PLEASE DO NOT RETURN YOUR FORM TO THE ABOVE ADDRESS.**

1. REPORT DATE AUGUST 2019		2. REPORT TYPE Final		3. DATES COVERED 1 MAY 2017 - 30 Apr 2019	
4. TITLE AND SUBTITLE Interrogating the Mechanism of Long Noncoding RNA ARlnc-1 in Regulating AR Signaling				5a. CONTRACT NUMBER W81XWH-17-1-0134	
				5b. GRANT NUMBER PC160970	
				5c. PROGRAM ELEMENT NUMBER	
6. AUTHOR(S) Yajia Zhang E-Mail: yajiazh@umich.edu				5d. PROJECT NUMBER	
				5e. TASK NUMBER	
				5f. WORK UNIT NUMBER	
7. PERFORMING ORGANIZATION NAME(S) AND ADDRESS(ES) Regents of the University of Michigan Ann Arbor, Michigan 48109				8. PERFORMING ORGANIZATION REPORT NUMBER	
9. SPONSORING / MONITORING AGENCY NAME(S) AND ADDRESS(ES) U.S. Army Medical Research and Materiel Command Fort Detrick, Maryland 21702-5012				10. SPONSOR/MONITOR'S ACRONYM(S)	
12. DISTRIBUTION / AVAILABILITY STATEMENT Approved for Public Release; Distribution Unlimited				11. SPONSOR/MONITOR'S REPORT NUMBER(S)	
				13. SUPPLEMENTARY NOTES	
14. ABSTRACT Prostate cancer is the most commonly diagnosed non-skin cancer in American men, causing an estimated 31,620 cases of death in 2019. Androgens and Androgen Receptor (AR) pathways play critical roles in development and functions of the prostate gland. They are also necessary for prostate cancer progression. As such, primary androgen deprivation therapies and second generation anti-androgen drugs offer clinical benefits for patients with metastatic disease. However, nearly all patients with metastatic castration-resistant prostate cancer (mCRPC) eventually develop resistance to these agents. Studies are thus warranted to discover novel players involved in the AR signaling pathway and in prostate cancer progression. To this end, we previously conducted transcriptome sequencing analysis to find long non-coding RNAs (lncRNAs) that are responsive to androgen stimulation, and are enriched in the process of prostate cancer progression. From this analysis, we identified lncRNA ARlnc1, which is directly regulated by AR, and has lineage-specific, cancer associated expression pattern in prostate tissues. Phenotypic effects after knocking down this lncRNA include delayed cell proliferation, increased apoptosis, and attenuated AR signaling. We observed a positive feedback loop between ARlnc1 and AR signaling. In this project, we interrogated the mechanisms through which ARlnc1 regulates AR signaling pathway. We discovered that ARlnc1 contributes to post-transcriptional regulation of AR transcript via RNA-RNA interaction. Moreover, ARlnc1 inhibition by antisense technologies delays prostate cancer growth in vitro and in vivo. Taken together, our findings support a role for ARlnc1 in maintaining AR signaling and identify ARlnc1 as a novel therapeutic target.					
15. SUBJECT TERMS Androgen Receptor, long non-coding RNA, ARlnc1					
16. SECURITY CLASSIFICATION OF: U			17. LIMITATION OF ABSTRACT Unclassified	18. NUMBER OF PAGES 40	19a. NAME OF RESPONSIBLE PERSON USAMRMC
a. REPORT Unclassified	b. ABSTRACT Unclassified	c. THIS PAGE Unclassified			19b. TELEPHONE NUMBER (include area code)

Table of Contents

	<u>Page</u>
1. Introduction.....	4
2. Keywords.....	4
3. Accomplishments.....	4
4. Impact.....	17
5. Changes/Problems.....	18
6. Products.....	18
7. Participants & Other Collaborating Organizations	19
8. Special Reporting Requirements.....	20
9. Appendices.....	20

1.INTRODUCTION:

Prostate cancer is the most commonly diagnosed non-skin cancer in American men, causing an estimated 31,620 cases of death in 2019. While the 5-year survival rate for men with low-grade prostate cancer is nearly 100%, for people diagnosed with advanced or metastasis disease, the 5-year survival rate is only ~30%. Androgens and Androgen Receptor (AR) pathways play critical roles in development and functions of the prostate gland. They are also necessary for prostate cancer progression. As such, primary androgen deprivation therapies and second generation anti-androgen drugs offer clinical benefits for patients with metastatic disease. However, nearly all patients with metastatic castration-resistant prostate cancer (mCRPC) eventually develop resistance to these agents. Studies are thus warranted to discover novel players involved in the AR signaling pathway and in prostate cancer progression. To this end, we previously conducted transcriptome sequencing analysis to find long non-coding RNAs (lncRNAs) that are responsive to androgen stimulation, and are enriched in the process of prostate cancer progression. From this analysis, we identified lncRNA ARlnc1, which is directly regulated by AR, and has lineage-specific, cancer associated expression pattern in prostate tissues. Phenotypic effects upon knocking down this lncRNA include delayed cell proliferation, increased apoptosis, and attenuated AR signaling. We observed a positive feedback loop between ARlnc1 and AR signaling. The purpose of this project is to interrogate the mechanisms through which ARlnc1 regulates AR signaling pathway.

2.KEYWORDS:

Androgen Receptor, long non-coding RNA, ARlnc1

3.ACCOMPLISHMENTS:

What were the major goals of the project?

The major goals of the project are to understand the mechanism through which ARlnc1 regulates AR signaling pathway, and to evaluate the therapeutic potential of modulating this interaction. We hypothesized that ARlnc1 regulates Androgen Receptor signaling through interaction with the AR transcript. Over the course of this grant, we have tested this hypothesis by a series of experiments, with the specific aims below:

(1) To characterize RNA-RNA interactions between ARlnc1 and AR transcripts *in vitro* and in cells.

(2) To investigate the molecular mechanism of ARlnc1 regulation on AR transcript stability.

(3) To evaluate the potential of ARlnc1-AR loop as a therapeutic target in pre-clinical models.

What was accomplished under these goals¹?

This section describes major activities, specific objectives, significant results/achievements, and discussion in the order of specific aims stated above.

Specific Aim 1: Characterizing RNA-RNA interactions between ARlnc1 and AR transcripts *in vitro* and in cells.

In our previous experiments, we have discovered Androgen Receptor (AR) as one of the targets that are significantly affected by ARlnc1. To find the molecular mechanism behind it, we utilized an *in silico* algorithm to predict RNA interactors of ARlnc1 (based on complementary base pair binding affinity). Interestingly, this approach identified 3' untranslated region (UTR) of AR mRNA as a potential binding partner. The objective here is to test whether this RNA-RNA interaction actually exist in cells.

We characterized interaction between ARlnc1 and AR transcripts using a series of biochemical assays and molecule labeling approaches. For *in vitro* experiments, we developed RNA-RNA binding assays, featured by RNA synthesis, BrU-labeled RNA pull down and qPCR analysis. To visualize this interaction in cells, we employed single molecule RNA-Fluorescent *in situ* hybridization (smFISH) to label transcripts in prostate cancer cell lines and tissues.

We first used synthesized RNAs to evaluate the relative binding affinity between AR 3'UTR and a panel of non-coding RNAs including ARlnc1. Compared to control RNAs (ARlnc1-antisense, LacZ, SChLAP1-antisense, THOR, and beads control), ARlnc1 binds with 1-980nt of AR-3'UTR with a higher affinity (**Figure 1a**). Next, to identify the sites on ARlnc1 that mediates this interaction, we constructed RNA fragments spanning every ~600bp of ARlnc1, and subsequently used these fragments for RNA-RNA binding assays. We discovered that the RNA fragment spanning 700-1300nt of ARlnc1 binds to AR 3'UTR with the highest affinity (**Figure 1b**), suggesting its critical role in mediating the interaction. In support of this observation, ARlnc1 RNA lacking nucleotides 700-1300 attenuates the binding between ARlnc1 and AR 3'UTR (**Figure 1c**).

¹ Some of the results presented in this final report have been included in the yearly progress report.

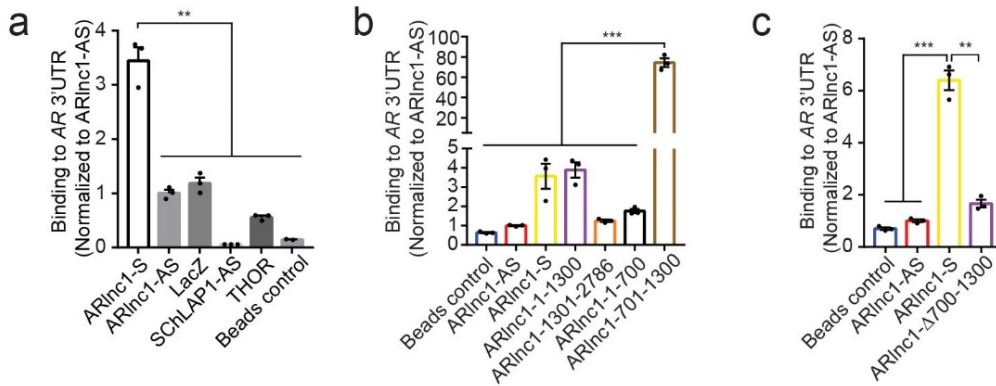


Figure 1: RNA-RNA interaction between ARInc1 and 3'UTR of AR transcript *in vitro*

(a) Relative binding between AR 3'UTR-1-980 RNA fragment and a panel of BrU-labeled RNAs, measured by *in-vitro* RNA-RNA interaction assay. Data were normalized to ARInc1-AS control. Mean \pm s.e.m. are shown, $n = 3$. $**P < 0.001$ by two-tailed Student's *t*-test.

(b) Relative binding between AR 3'UTR-1-980 RNA and a panel of BrU labeled RNA fragments spanning ARInc1. Data were normalized to ARInc1-AS control. Mean \pm s.e.m. are shown, $n = 3$. $***$ Adjusted $P = 0.0001$, determined by ANOVA with Dunnett's multiple comparisons test.

(c) Relative binding between AR 3'UTR-1-980 RNA and ARInc1 with 700-1300 deletion, measured by *in-vitro* RNA-RNA interaction assay. Data were normalized to ARInc1-AS control. Mean \pm s.e.m. are shown, $n = 3$. $***P = 0.0001$, $**P = 0.0003$ by two-tailed Student's *t*-test.

To determine whether ARInc1 and AR transcripts are associated with each other in cells, we developed single molecule RNA-fluorescent *in situ* hybridization (smFISH) to label and visualize specific transcripts. In AR-positive prostate cancer cell model MDA-PCa-2b, we observed co-localization of endogenous ARInc1 and AR transcripts (**Figure 2a**). The co-localization rate between these two transcripts were significantly higher compared to those between ARInc1 and abundantly-expressed control RNAs (**Figure 2b**).

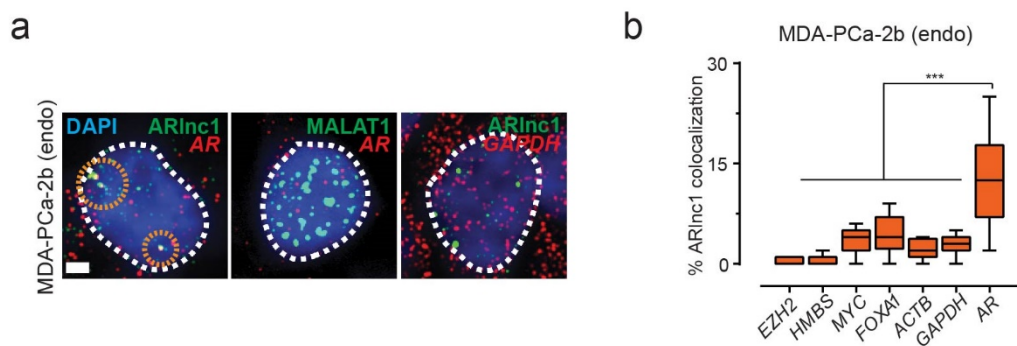


Figure 2: Co-localization of ARInc1 and AR transcripts in MDA-PCa-2b cells, depicted by single molecule fluorescent *in situ* hybridization (smFISH).

(a) Representative pseudocolored images of MDA-PCa-2b cell nuclei stained for the indicated endogenous (endo) transcripts and DAPI. Scale bar, 5 μm . Orange circles represent regions of colocalization.

(b) Quantification of the percentage of ARInc1 molecules co-localizing with a panel of mRNAs, respectively. Center line and whiskers depict the median and range respectively and box extends from 25th to 75th percentiles ($n = 50$ cells for each sample aggregated from 3 independent experiments). *** $P < 0.0001$ by two-tailed Student's t -test.

To further validate the RNA-RNA interaction sites identified *in vitro*, we employed an exogenous system, where U2-OS cells were co-transfected with AR-expression construct and constructs encoding varied ARInc1-fragments. ARInc1 fragments with 700-1300nt co-localized with AR at a higher rate, compared to fragments lacking this region (**Figure 3**).

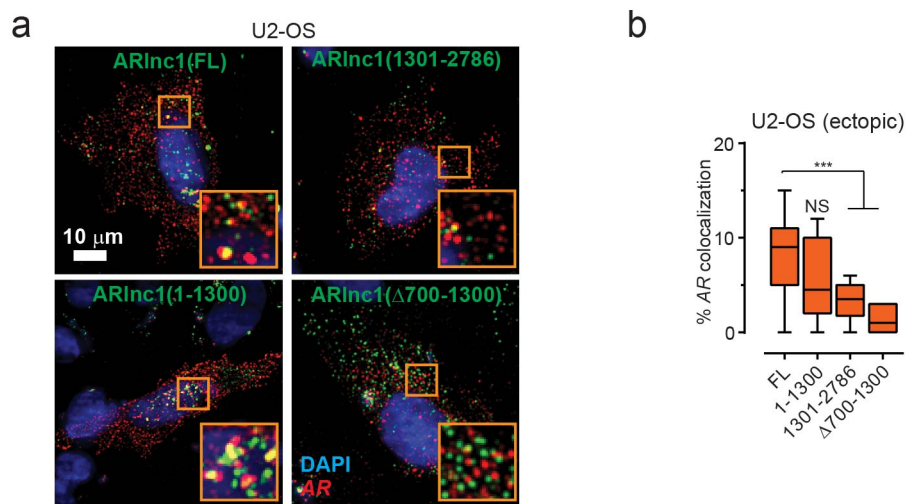


Figure 3: Co-localization of ARInc1 fragments and AR transcripts exogenously expressed in U2-OS cells, depicted by single molecule fluorescent *in situ* hybridization (smFISH).

(a) Representative pseudo-colored images of U2-OS cells stained for DAPI (nucleus), indicated fragments of ARInc1 and AR transcripts (smFISH). Scale bar, 10 μm . Inset, 10x10 μm^2 zoomed-in view of orange box in the image.

(b) Quantification of the percent of AR molecules colocalizing with various ARInc1 fragments. Center line and whiskers depict the median and range respectively and box extends from 25th to 75th percentiles ($n = 50$ cells for each sample aggregated from 3 independent experiments). *** $P < 0.0001$ by two-tailed Student's t -test. NS: not significant.

Finally, to explore whether co-localization between ARInc1 and AR exist in tissues, we performed smFISH on AR-positive prostate cancer tissue samples. A significantly higher co-localization rate was observed between AR and ARInc1 transcripts, compared

to the co-localization rate between AR and abundantly-expressed HMBS transcripts (**Figure 4**).

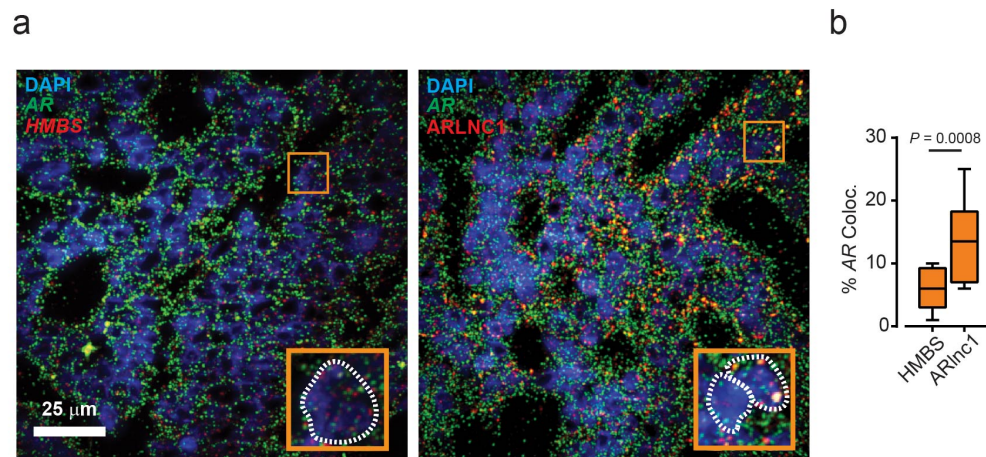


Figure 4: Co-localization of ARlnc1 and AR transcripts in prostate cancer tissue samples

(a) Representative pseudo-colored images of ARlnc1 positive prostate cancer tissues stained with DAPI (nucleus) and AR, HMBS or ARlnc1 transcripts (smFISH). Scale bar, 25 μm . Inset, 5.5x5.5 μm^2 zoomed-in view of box within large panel.

(b) Quantification of the percentage of AR molecules colocalizing with HMBS or ARlnc1 is depicted in box plot. Center line and whiskers depict the median and range respectively and box extends from 25th to 75th percentiles ($n = 15$ field-of-views aggregated for each sample aggregated from 3 independent tissues). $**P < 0.001$ by two-tailed Student's t -test.

Specific Aim 2: Investigating the molecular mechanism of ARlnc1 regulation on AR transcript stability.

Having established the interaction between ARlnc1 and AR transcripts *in vitro*, in cells, and in tissue samples, we next sought to investigate how ARlnc1 functions to affect AR transcript stability. To achieve this, we conducted reporter gene analysis of AR 3'UTR under control or ARlnc1-knockdown conditions. We further investigated whether HuR (ELAV1), a known protein that affects AR 3'UTR activity, is involved in ARlnc1 regulation of AR. We also utilized antisense oligonucleotides to disrupt interaction sites between ARlnc1 and AR, and recorded changes on RNA-RNA co-localization and on AR signaling.

Dual luciferase assay was conducted using an AR 3'UTR reporter construct containing 3.2kb of AR 3'UTR in front of a luciferase reporter. AR-positive prostate cancer cells were co-transfected with AR 3'UTR reporter construct and siRNAs targeting ARlnc1. As shown in **Figure 5**, ARlnc1 knockdown significantly reduced AR 3'UTR luciferase activity.

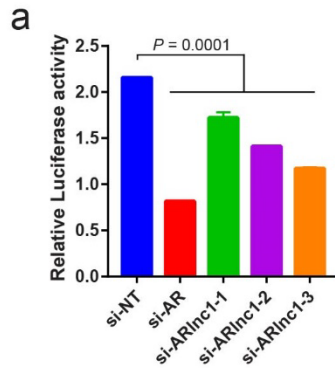


Figure 5: Relative luciferase activity of AR 3'UTR following treatments of non-targeting siRNA, or siRNA targeting AR 3'UTR region (positive control), or siRNAs targeting ARInc1. $n = 5$, P value calculated from ANOVA.

Next, we asked the question whether this phenotype is achieved through HuR (ELAV1), a known RNA-binding protein that mediates AR transcript stability. We performed reciprocal interaction assays between ARInc1 and HuR protein *in vitro* (**Figure 6a, 6b**). The results suggested dose-dependent binding affinity between HuR protein and synthesized ARInc1 RNA. Further assays of RNA-immunoprecipitation (RIP) using HuR antibody confirmed this interaction in cells (**Figure 6c**). We also confirmed the reported interaction between HuR and AR transcript by RIP (**Figure 6d**). Interestingly, the AR-HuR interaction could be affected by ARInc1. This is indicated by a decreased relative binding between HuR and AR following ARInc1 loss (**Figure 6d**).

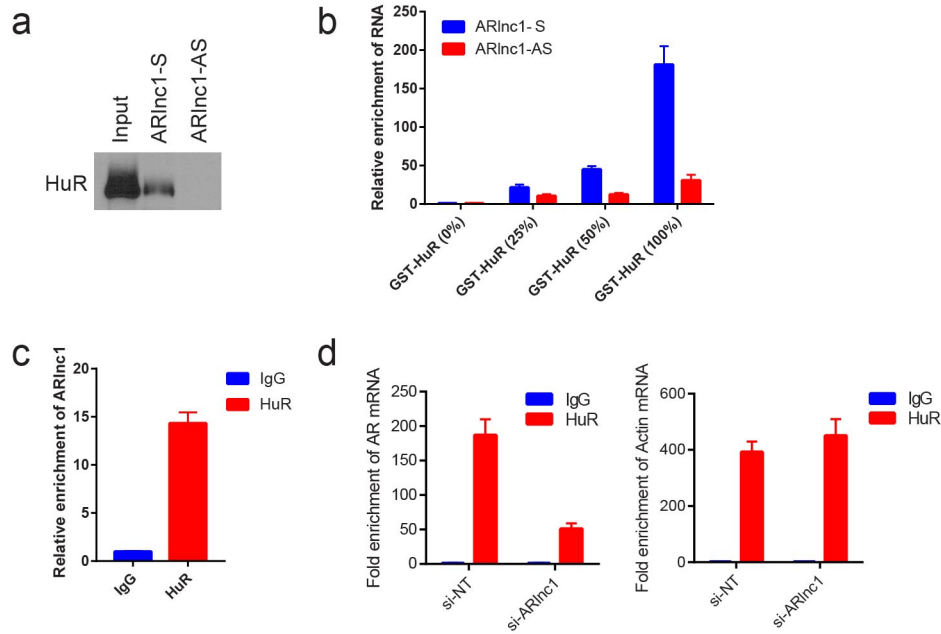


Figure 6: Binding between HuR and ARlnc1

- (a) Relative binding between HuR protein and ARlnc1-S or ARlnc1-AS RNA *in vitro*, evaluated by western blotting following RNA-pull-down.
- (b) Dose-dependent binding between ARlnc1 and GST-HuR, following GST-pull down. Relative RNA enrichment was assessed by qPCR analysis.
- (c) RNA immune-precipitation followed by qPCR analysis to detect binding between HuR protein and ARlnc1 in MDA-PCa-2b cells.
- (d) Relative binding between HuR protein and AR transcripts or ACTB transcripts, under control or ARlnc1-knockdown condition. Binding was quantified by RIP-qPCR analysis in MDA-PCa-2b cells.

We next asked whether the physical co-localization between AR and ARlnc1 results in functional regulation of AR transcript and AR signaling. We utilized antisense oligonucleotides (ASOs) to interfere with the identified RNA-RNA binding sites in cells. Using RNA interaction assays and smFISH assays, we confirmed the ability of ASOs to disrupt interactions between ARlnc1 and AR *in vitro* and in cell lines (**Figure 7**). Transfection of these blocking ASOs into cells resulted in attenuated AR signaling, as well as modest decrease of AR transcript (**Figure 8**).

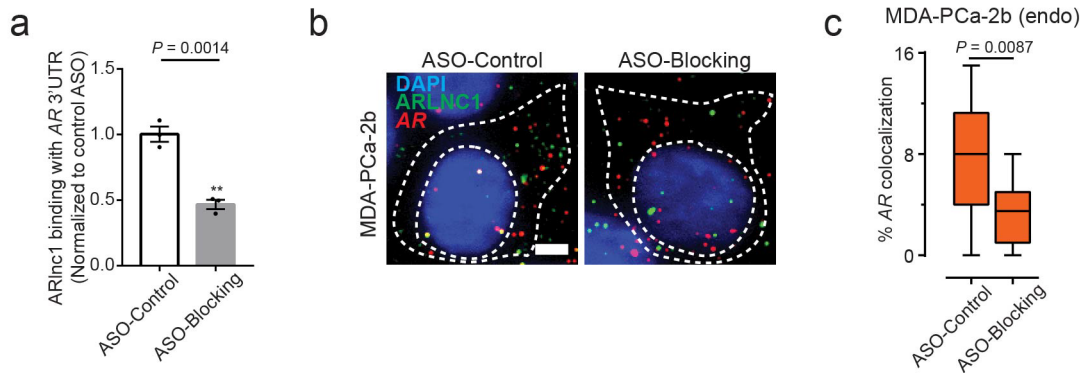


Figure 7: Blocking ASOs disrupt ARlnc1-AR interaction *in vitro* and in cells.

(a) ASOs targeting nucleotides 700–1300 on the ARlnc1 transcript (ASO-blocking) inhibit ARlnc1 interaction with the AR 3' UTR. *In vitro* RNA–RNA interaction assays were performed using ARLNC1 and the AR 3' UTR, with the addition of the blocking ASO pool or control ASO. Data were normalized to the control ASO.

(b) smFISH showing that ASOs targeting 700-1300nt on ARlnc1 transcript (ASO-Blocking) inhibit ARlnc1 colocalization with AR *in situ*.

(c) Quantification of the percent of AR transcripts co-localizing with ARlnc1 after various treatments in MDA-PCa-2b cells. Center lines and whiskers depict the median and range and box extends from 25th to 75th percentiles ($n = 50$ cells for each sample aggregated from 3 independent experiments).

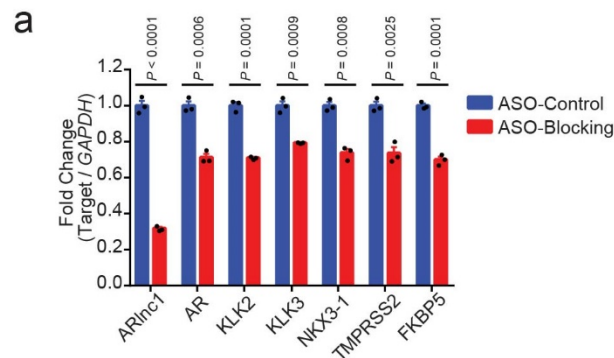


Figure 8: Effect of blocking ASOs on AR signaling in MDA-PCa-2b cells

(a) qPCR analysis of ARlnc1, AR and AR signaling genes (KLK2, KLK3, NKX3-1, TMPRSS2 and FKBP5) in MDA-PCa-2b cells transfected with control or blocking ASOs targeting the interaction site between ARlnc1 and the AR 3' UTR.

Specific Aim 3: Evaluating the potential of ARlnc1-AR loop as a therapeutic target in pre-clinical models.

Our preliminary data showed that ARlnc1 regulates AR signaling in a feed-forward loop. The goal of this aim is to test whether ARlnc1 can be developed into a therapeutic target in prostate cancers with sustained AR signaling. We employed shRNAs and antisense oligonucleotides to evaluate antitumor phenotypes of ARlnc1 knockdown in a series of preclinical models.

We generated MDA-PCa-2b cells and LNCaP-AR cells expressing non-targeting shRNA or shRNAs targeting ARlnc1. Cell proliferation was monitored in mono-layered cultures, or in cell line derived xenografts implanted in mice. In both growing conditions, ARlnc1 knockdown significantly delays cancer cell growth. This observation was in accord with previous results generated following siRNA-mediated knockdown of ARlnc1.

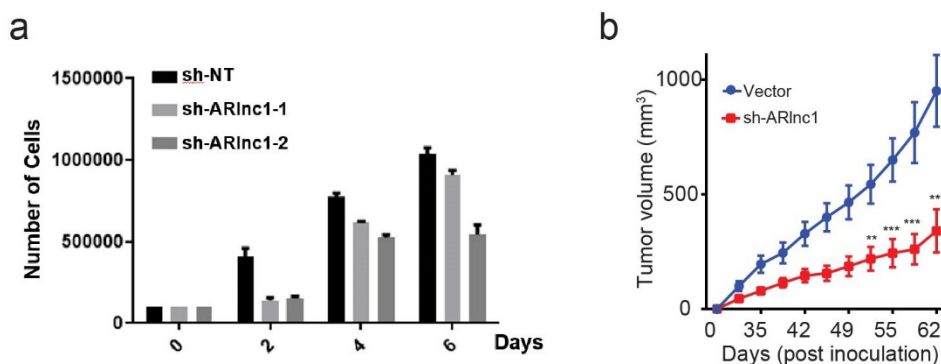


Figure 9: Inhibition of ARlnc1 by shRNA delays prostate cancer cell growth

(a) Counts of MDA-PCa-2b cells over the course of 6 days following treatment of control shRNA, or shRNA targeting ARlnc1.

(b) Tumor growth of LNCaP-AR cells expressing shRNA targeting ARLNC1 or shRNA vector. Mean \pm s.e.m. values are shown. $n = 10$ independent tumors, *** $P < 0.0001$, ** $P = 0.0007$, determined by two-tailed Student's t test.

Antisense oligonucleotides (ASOs) have emerged as a novel approach to inhibit RNA targets, through mechanisms of RNase H degradation, modulating RNA splicing or translation. We hypothesized that ASOs targeting ARlnc1 are able to decrease ARlnc1 expression in pre-clinical models, thus inhibiting prostate cancer cell growth. To test this hypothesis, we transfected ARlnc1 ASOs into MDA-PCa-2b cells, profiled gene expression changes, and monitored cancer cell growth. We observed that ARlnc1 ASOs induced similar gene expression changes, compared to ARlnc1 siRNAs (**Figure 10a**). Cells transfected with ARlnc1 ASOs grew slower than those treated with control ASOs

(Figure 10b). This phenotype was specific to AR-positive prostate cancer cells, not AR signaling-negative cell line models (Figure 10c).

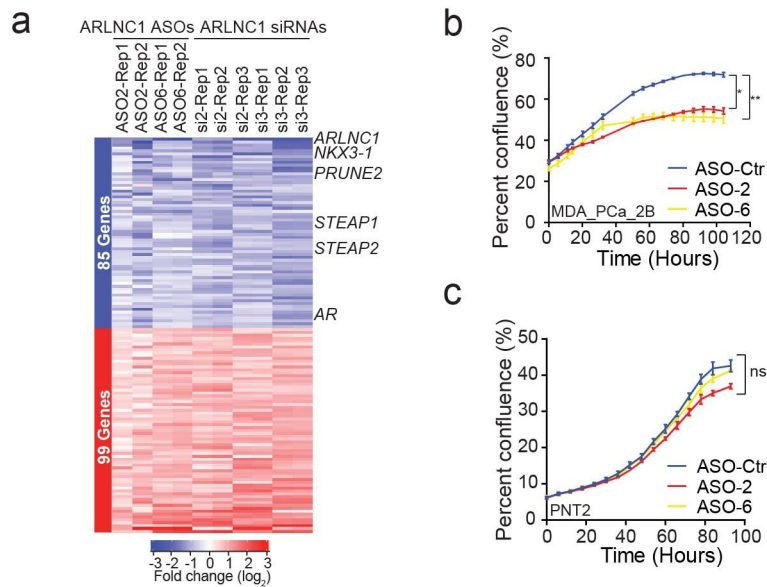


Figure 10: Treatment of ARInc1 ASO inhibits cell growth

(a) Gene expression profiling for siRNA-mediated or ASO-mediated ARLNC1 knockdown in MDA-PCa-2b cells. The numbers above the heat map represent the specific microarray replicates.

(b-c) Transfection of ASOs targeting ARLNC1 in AR-positive MDA-PCa-2b cells inhibits cell proliferation. The AR-negative prostate cell line PNT2 serves as a negative control. Mean \pm s.e.m. values are shown, $n = 6$, $*P$ (adjusted) = 0.0112, $**P$ (adjusted) = 0.0065, NS: not significant; compared to the control-ASO group.

Since we planned to use ASOs on tumor xenograft models in mice, we next tested ASO delivery efficacy in cell sphere models, without using lipid-based transfection reagents. We generated three-dimensional MDA-PCa-2b cell spheres, and incubated them with either control ASOs, or ARInc1 ASOs. As shown in **Figure 11**, free-uptake treatment of ARInc1 ASOs attenuates target expression, and inhibits MDA-PCa-2b cell proliferation.

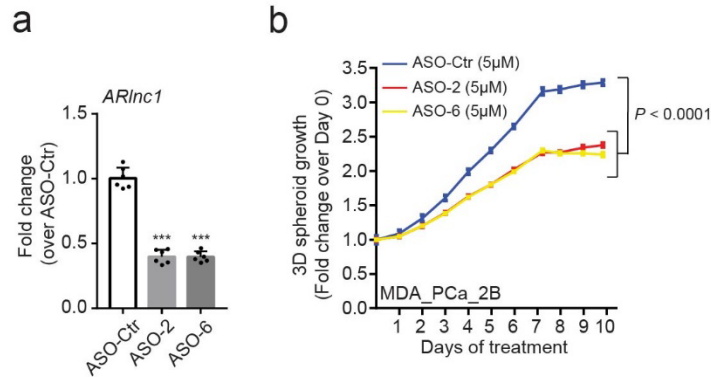


Figure 11: ARInc1 ASOs inhibit cell growth in 3D-sphere models

(a-b) Free-uptake treatment of ARInc1 ASOs inhibits MDA-PCa-2b cell proliferation in the 3D sphere models. Cells were harvested at the end of the experiment, and ARInc1 expression was evaluated by qPCR analysis. Mean \pm s.d. values are shown, $n = 6$. $***P < 0.0001$ compared to control-ASO-treated cells, by two-tailed Student's t test.

Finally, we evaluated the therapeutic potential of these ASOs *in vivo*. We developed cell-line derived xenografts by subcutaneously implanting MDA-PCa-2b cells suspended in Matrigel scaffolds. When the mean tumor volume reached approximately 150 mm^3 , mice were randomized into two groups and treated with ARInc1-specific or control ASO. ASOs were subcutaneously injected at 50 mg per kg body weight, with dosing scheme of 5d on/2d off. When the average tumor size in the control group reached $1,500 \text{ mm}^3$, mice were euthanized and the primary tumors were excised for weight determination.

We observed significant delay of tumor growth following ARInc1 ASO treatment (**Figure 12a-b**). Cell proliferation rate is lower when ARInc1 was inhibited, as demonstrated by Ki-67 staining (**Figure 12c**). Another evidence of on-target effect was the decreased AR signaling following ARInc1 loss (**Figure 12d**).

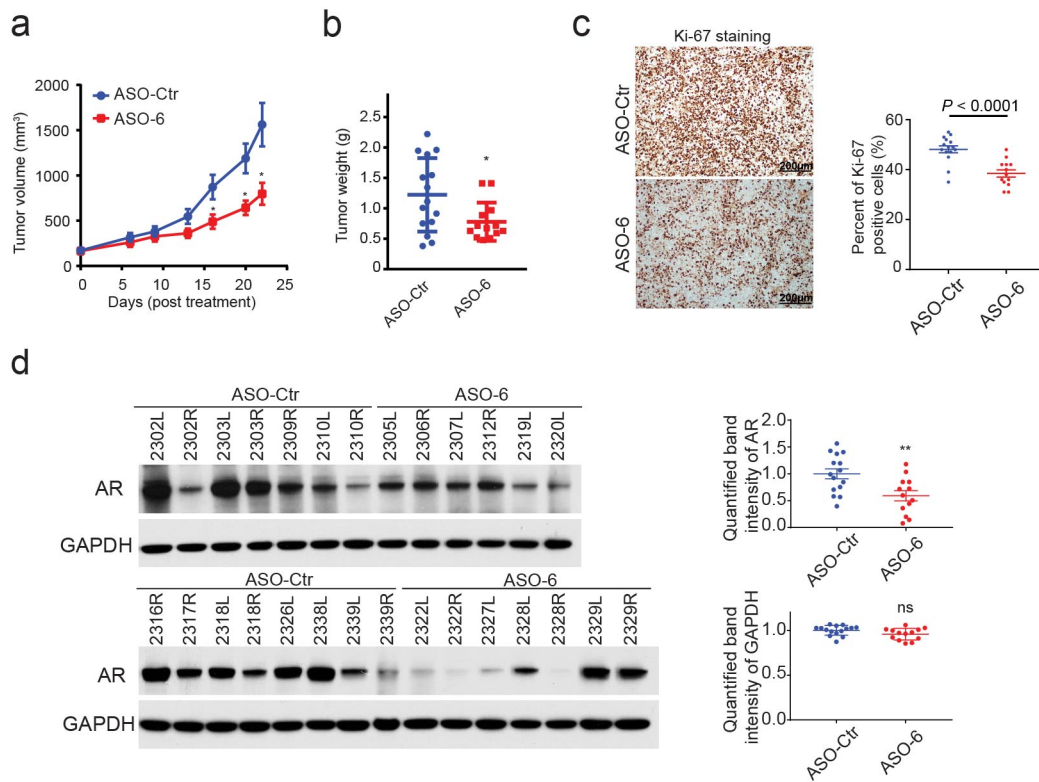


Figure 12: ARInc1 ASOs inhibit prostate cancer growth in cell-line derived xenografts

(a-b) Effect of ASO treatment on the growth of MDA-PCa-2b xenografts in male athymic nude mice, with control ASO or ARInc1 ASO treatment subcutaneously at 50 mg per kg body weight, five times per week for 3 weeks. Tumors were measured by caliper biweekly (a) and tumor weights were measured at the end point (b). Mean \pm s.d. values are shown. $*P = 0.0251$, $***P < 0.0001$; compared to control ASO by two-tailed Student's *t* test.

(c) Left, immunohistochemistry staining for Ki67 in MDA-PCa-2b xenograft treated with control ASO or ASO against ARInc1. Right, summary of Ki67 tumor staining for control or ARInc1-ASO-treated tumors shows significant difference in Ki67 staining intensity.

(d) Left, immunoblots of AR and GAPDH in MDA-PCa-2b xenografts treated with control ASO or ASO targeting ARInc1. Right, the relative intensity of the bands was quantified using Image J. Mean \pm s.e.m. values are shown. $**P < 0.005$; ns, not significant; compared to the control-ASO-treated group by two-tailed Student's *t* test.

Overall, during the course of this grant, we have interrogated the mechanism of long non-coding RNA ARInc1 in regulating AR signaling. Specifically, we demonstrated that ARInc1 associates with AR transcript in cells. This RNA-RNA interaction is at least partially involved in ARInc1 regulation on AR transcript stability and downstream AR

signaling. ARInc1 has the potential to be not only a mechanistic biomarker but also a therapeutic target for advanced prostate cancer.

What opportunities for training and professional development has the project provided?

Over the course of this Early Investigator Research Award, I was offered many opportunities for training, education and professional development. These activities range from attending RNA Innovation seminars at University of Michigan, to giving poster presentations at nationwide conferences. Details of these opportunities are listed below:

Training and education:

(1) I presented research updates and plans at the thematic meetings and lab meetings to the entire research group. Feedbacks received from my mentor and other research investigators largely advanced my research.

(2) I had bi-weekly one-on-one meetings with my mentor. During these meetings, I had in-depth discussion with my mentor regarding problems I came across and possible ways to solve them. He also offered insights and suggestions on possible research directions.

(3) I routinely attended the department seminars, which include the Pathology Department weekly seminar and the RNA Innovation seminars at University of Michigan.

(4) I completed my PhD training in Molecular and Cellular Pathology at the end of the reporting period. Meanwhile, by continuing to take required courses throughout the past five years, I also got a Master degree in Bioinformatics. My experimental skills in molecular biology, plus the analytic skills in Bioinformatics, have made me better prepared for leading independent research projects in future.

Poster presentations at scientific conferences:

I attended several meetings and presented part of the data collected here on posters.

(1) Prostate Specialized Programs of Research Excellence (SPORE) Annual Meeting Feb. 2018, Ft. Lauderdale, Florida.

(2) AACR Annual meeting, Apr. 2018, Chicago, Illinois.

Talks at scientific conferences:

I was invited or selected by abstract to give talks at campus-wide or nation-wide conferences. These opportunities allowed me to communicate with fellow scientists and to receive feedbacks on lncRNA research. I developed skills of preparing and giving presentations, and learned to deliver scientific concepts in a clear and effective manner.

(1) 16th Annual Pathology Research Symposium, Nov. 2017, University of Michigan

(2) AACR Annual meeting (Mini-symposia: Noncoding RNAs in Cancer Biology), Apr. 2019, Atlanta, Georgia.

Mentoring experience:

I helped with training several undergraduate research volunteers and technicians in our lab. Specifically, I introduced to them ways to approach scientific questions, taught them experimental techniques, and helped them with preparing research presentations.

How were the results disseminated to communities of interest?

Nothing to Report

What do you plan to do during the next reporting period to accomplish the goals?

Nothing to report.

4.IMPACT:

What was the impact on the development of the principal discipline(s) of the project?

Past studies on AR signaling has largely focused on protein coding genes. Examples of de-regulated AR signaling in metastatic prostate cancer include AR amplifications, AR mutations, AR splicing variants, and activation of the AR via ligand-independent ways, etc. In this project, we studied the mechanisms of how non-coding RNAs are involved in AR signaling regulation. We demonstrated that lncRNA could modulate transcript stability in cells via RNA-RNA interaction and co-localization. Moreover, functional mechanism and therapeutic potential of oncogenic non-coding RNAs could be effectively evaluated by antisense technologies. In addition, the experimental approaches developed here, which include RNA-RNA interaction assay, smFISH assay, and antisense technologies, could be utilized for other lncRNA research projects in future.

What was the impact on other disciplines?

Nothing to Report.

What was the impact on technology transfer?

Nothing to Report.

What was the impact on society beyond science and technology?

Nothing to Report.

5.CHANGES/PROBLEMS:

Nothing to Report.

6.PRODUCTS:

Publications, conference papers, and presentations

(Reporting only the major publication(s) resulting from the work under this award)

▪ Journal publications.

Yajia Zhang*, Sethuramasundaram Pitchiaya*, Marcin Cieřlik*, Yashar S. Niknafs, Jean C-Y.Tien, Yasuyuki Hosono, Matthew K. Iyer, Sahr Yazdani, Shruthi Subramanyam, Sudhanshu K. Shukla, Xia Jiang, Lisha Wang, Tzu-Ying Liu, Michael Uhl, Alexander Gawronski, Yuanyuan Qiao, Lanbo Xiao, Saravana M. Dhanasekaran, Kristin M. Juckette, Lakshmi P. Kunju, Xuhong Cao, Utsav Patel, Mona Batish, Girish C. Shukla, Michelle T. Paulsen, Mats Ljungman, Hui Jiang, Rohit Mehra, Rolf Backofen, Cenk S. Sahinalp, Sue Freier, Andy Watt, Shuling Guo, John T. Wei, Felix Y. Feng, Rohit Malik#, Arul M. Chinnaiyan#. **Analysis of the androgen receptor-regulated lncRNA landscape identifies a role for ARLNC1 in prostate cancer progression.** *Nature Genetics*, May 28, 2018, doi: 10.1038/s41588-018-0120-1

▪ Other publications, conference papers, and presentations.

Poster presentation and Abstract: **Yajia Zhang**, Sethuramasundaram Pitchiaya, Marcin Cieřlik, Yashar S. Niknafs, Jean C-Y. Tien, Yasuyuki Hosono, Matthew K. Iyer, Lisha Wang, Yuanyuan Qiao, Xuhong Cao, Mats Ljungman, Hui Jiang, Rohit Mehra, Shuling Guo, John T. Wei, Felix Y. Feng, Rohit Malik, Arul M. Chinnaiyan. **The Androgen Receptor-Regulated lncRNA Landscape Reveals a Role for ARlnc1 in Prostate Cancer Progression.** [abstract 2458]. In: *Proceedings of the 109th Annual Meeting of the American Association for Cancer Research*; 2018 Apr 14-18; Chicago, IL, AACR.

Poster: **Yajia Zhang**, Rohit Malik, Marcin Cieslik, Sethuramasundaram Pitchiaya, Jean Ching-Yi Tien, Yashar Niknafs, Yasuyuki Hosono, Sahr Yazdani, Xuhong Cao, Dan Robinson and Arul Chinnaiyan. **Investigating the role of androgen receptor regulated long non-coding RNA ARlnc1 in prostate cancer.** *Keystone Symposia Conference- Noncoding RNAs: From Disease to Targeted Therapeutics*, 2017

7. PARTICIPANTS & OTHER COLLABORATING ORGANIZATIONS

What individuals have worked on the project?

Name:	<i>Yajia Zhang</i>
Project Role:	<i>Graduate Student</i>
Researcher Identifier (e.g. ORCID ID):	<i>N/A</i>
Nearest person month worked:	<i>6</i>
Contribution to Project:	<i>Ms. Zhang has performed work in the area of prostate cancer biology, especially discovering functioning mechanism of long non-coding RNAs in cancer context.</i>
Funding Support:	<i>N/A</i>

Has there been a change in the active other support of the PD/PI(s) or senior/key personnel since the last reporting period?

Nothing to report.

What other organizations were involved as partners?

▪ **Organization Name:**

Ionis Pharmaceuticals, Inc

▪ **Location of Organization:**

2855 Gazelle Court Carlsbad, CA 92010

▪ **Partner's contribution to the project**

▪ **In-kind support:** They helped with designing and synthesis of clinical-grade antisense oligonucleotides that were used for lncRNA inhibition.

8.SPECIAL REPORTING REQUIREMENTS

Nothing to report.

9.APPENDICES:

(1) curriculum vitae

(2) Journal publication:

Yajia Zhang*, Sethuramasundaram Pitchiaya*, Marcin Cieřlik*, Yashar S. Niknafs, Jean C-Y.Tien, Yasuyuki Hosono, Matthew K. Iyer, Sahr Yazdani, Shruthi Subramanyam, Sudhanshu K. Shukla, Xia Jiang, Lisha Wang, Tzu-Ying Liu, Michael Uhl, Alexander Gawronski, Yuanyuan Qiao, Lanbo Xiao, Saravana M. Dhanasekaran, Kristin M. Juckette, Lakshmi P. Kunju, Xuhong Cao, Utsav Patel, Mona Batish, Girish C. Shukla, Michelle T. Paulsen, Mats Ljungman, Hui Jiang, Rohit Mehra, Rolf Backofen, Cenk S. Sahinalp, Sue Freier, Andy Watt, Shuling Guo, John T. Wei, Felix Y. Feng, Rohit Malik#, Arul M. Chinnaiyan#. **Analysis of the androgen receptor-regulated lncRNA landscape identifies a role for ARLNC1 in prostate cancer progression.** *Nature Genetics*, May 28, 2018, doi: 10.1038/s41588-018-0120-1

Yajia Zhang

Research Fellow
Michigan Center for Translational Pathology
University of Michigan

5121 Rogel Cancer Center
1500 East Medical Center Drive

Education

- 9/2013 - 8/2019 Ph.D. in Molecular and Cellular Pathology,
University of Michigan Medical School, Ann Arbor, Michigan, USA
- 9/2017 - 5/2019 M.S. in Bioinformatics,
University of Michigan Medical School, Ann Arbor, Michigan, USA
- 9/2009 - 6/2013 B.S. in Biological Science,
Nankai University, Tianjin, China

Working Experience

- 8/2019 - current Research Fellow,
Michigan Center for Translational Pathology, Ann Arbor, MI, USA
- 9/2013 - 5/2019 Graduate Student Research Assistant,
University of Michigan, Ann Arbor, MI, USA
Rotation Advisors: Scott A. Tomlins, MD, PhD, Shawn Xu, PhD
Thesis Advisor: Arul M. Chinnaiyan, MD, PhD
- 9/2011 - 6/2013 Undergraduate Student Research Assistant,
Nankai University, School of Life Sciences, Tianjin, China

Awards & Honors

- 2019 Rackham Conference Travel Grant
- 2019 Invited speaker, American Association of Cancer Research Annual Meeting 2019
- 2018 Rackham Conference Travel Grant
- 2017 Department of Defense- FY16 Prostate Cancer Research Program- Early Investigator Research Award
- 2017 Rackham International Conference Travel Grant
- 2014 Research Day Abstract Award, 5th Annual Anatomic, Molecular, Hematopathology Research

- Day at University of Michigan (Project: Targeted next generation sequencing of epithelioid angiomyolipoma identifies germline BRCA2 variants in young patients)
- 2012 First Prize of Excellent Undergraduate Scholarship of Nankai University
- 2012 Creative Research Award for the Undergraduates of Nankai University (Third Prize)
- 2010 *Kechang Wang* Scholarship
- 2009 Excellent Freshman Scholarship of Nankai University

Published Works

- [1] **Yajia Zhang***, Sethuramasundaram Pitchiaya*, Marcin Cieřlik*, Yashar S. Niknafs, Jean C-Y.Tien, Yasuyuki Hosono, Matthew K. Iyer, Sahr Yazdani, Shruthi Subramanyiam, Sudhanshu K. Shukla, Xia Jiang, Lisha Wang, Tzu-Ying Liu, Michael Uhl, Alexander Gawronski, Yuanyuan Qiao, Lanbo Xiao, Saravana M. Dhanasekaran, Kristin M. Juckette, Lakshmi P. Kunju, Xuhong Cao, Utsav Patel, Mona Batish, Girish C. Shukla, Michelle T. Paulsen, Mats Ljungman, Hui Jiang, Rohit Mehra, Rolf Backofen, Cenk S. Sahinalp, Sue Freier, Andy Watt, Shuling Guo, John T. Wei, Felix Y. Feng, Rohit Malik#, Arul M. Chinnaiyan#. **Analysis of the androgen receptor-regulated lncRNA landscape identifies a role for ARLNC1 in prostate cancer progression.** *Nature Genetics*, May 28, 2018, doi: 10.1038/s41588-018-0120-1
- [2] Josh N. Vo, Marcin Cieslik, **Yajia Zhang**, Sudhanshu Shukla, Lanbo Xiao, Yuping Zhang, Yi-Mi Wu, Saravana M. Dhanasekaran, Carl G. Engelke, Xuhong Cao, Dan R. Robinson, Alexey I. Nesvizhskii, Arul M. Chinnaiyan. **The Landscape of Circular RNA in Cancer.** *Cell*, February 7, 2019, DOI: <https://doi.org/10.1016/j.cell.2018.12.021>.
- [3] Lanbo Xiao, Jean C Tien, Josh Vo, Mengyao Tan, Abhijit Parolia, **Yajia Zhang**, Lisha Wang, Yuanyuan Qiao, Sudhanshu Shukla, Xiaojun Wang, Heng Zheng, Fengyun Su, Xiaojun Jing, Esther Luo, Andrew Delekta, Kristin M Juckette, Alice Xu, Xuhong Cao, Ajjai S Alva, Youngsoo Kim, A Robert MacLeod, Arul M Chinnaiyan. **Epigenetic reprogramming with antisense oligonucleotides enhances the effectiveness of androgen receptor inhibition in castration-resistant prostate cancer.** *Cancer Research*, 78(20), 5731–40, 2018.
- [4] Alexander R. Gawronski, Michael Uhl, **Yajia Zhang**, Yen-Yi Lin, Yashar S. Niknafs, Varune R. Ramnarine, Rohit Malik, Felix Feng, Arul M. Chinnaiyan, Colin C. Collins, S. Cenk Sahinalp, Rolf Backofen. **MechRNA: prediction of lncRNA mechanisms from RNA–RNA and RNA–protein interactions.** *Bioinformatics*, Apr 03, 2018, <https://doi.org/10.1093/bioinformatics/bty208>
- [5] Andrew S. McDaniel, Daniel H. Hovelson, Andi K. Cani, Chia-Jen Liu, Yali Zhai, **Yajia Zhang**, Alon Z. Weizer, Rohit Mehra, Felix Y. Feng, Ajjai S. Alva, Todd M. Morgan, Jeffrey S. Montgomery, Javed Siddiqui, Seth Sadis, Santhoshi Bandla, Paul D. Williams, Kathleen R. Cho, Daniel R. Rhodes, Scott A. Tomlins. **Genomic profiling of penile squamous cell carcinoma reveals new opportunities for targeted therapy.** *Cancer Research*, Dec 15, 2015, 75(24): 5219-27
- [6] Jing Li*, Weichao Wang*, **Yajia Zhang**, Marcin Cieřlik, Jipeng Guo, Mengyao Tan, Michael D. Green, Tomek Maj, Weimin Wang, Wei Li, Gaopeng Li, Lili Zhao, Benjamin Bitler, Theodore S. Lawrence, Rugang Zhang, Kathleen Cho, Yali Dou, Ilona Kryczek, David Huntsman, Arul M. Chinnaiyan, Weiping Zou.

ARID1A genetic status drives cancer immune phenotype and affects immunotherapy. *Immunity*, (under revision)

Conference Presentations

Invited talk: **Yajia Zhang**, Lanbo Xiao, Mengyao Tan, Yasuyuki Hosono, Arul Chinnaiyan. **Functional CRISPR screen towards identifying novel conserved long non-coding RNAs with oncogenic activity. *110th Annual Meeting of the American Association for Cancer Research*; Atlanta, GA, 2019**

Poster: **Yajia Zhang**, Sethuramasundaram Pitchiaya, Marcin Cieřlik, Yashar S. Niknafs, Jean C-Y. Tien, Yasuyuki Hosono, Matthew K. Iyer, Lisha Wang, Yuanyuan Qiao, Xuhong Cao, Mats Ljungman, Hui Jiang, Rohit Mehra, Shuling Guo, John T. Wei, Felix Y. Feng, Rohit Malik, Arul M. Chinnaiyan. **The Androgen Receptor-Regulated LncRNA Landscape Reveals a Role for ARlnc1 in Prostate Cancer Progression. *109th Annual Meeting of the American Association for Cancer Research*; Chicago, IL, 2018**

Poster: **Yajia Zhang**, Rohit Malik, Marcin Cieslik, Sethuramasundaram Pitchiaya, Jean Ching-Yi Tien, Yashar Niknafs, Yasuyuki Hosono, Sahr Yazdani, Xuhong Cao, Dan Robinson and Arul Chinnaiyan. **Investigating the role of androgen receptor regulated long non-coding RNA ARlnc1 in prostate cancer. *Keystone Symposia Conference- Noncoding RNAs: From Disease to Targeted Therapeutics*; Banff, Canada; 2017**

Poster: **Yajia Zhang**, Rohit Malik, Jean Tien, Christine Brennan, Beth Lawlor, Arul Chinnaiyan. **Targeting EWSR1 as a therapeutic method to treat Ewing Sarcoma *Molecular and Cellular Pathology Annual Symposium*; University of Michigan; 2015**

Platform talk and poster presentation: **Yajia Zhang**, Anmol Amin, Venkata Yadati, Andi Cani, Chia-Jen Liu, Michael J. Quist, Andrew McDaniel, Catherine S. Grasso, Scott A. Tomlins **Targeted next generation sequencing of epithelioid angiomyolipoma identifies germline BRCA2 variants in young patients *5th Annual Anatomic, Molecular, Hematopathology Research Day*; University of Michigan; 2014**

Review for journals

Frontiers in Oncology, Scientific Reports, Medicine, Journal of Cancer Therapy

Analysis of the androgen receptor–regulated lncRNA landscape identifies a role for ARLNC1 in prostate cancer progression

Yajia Zhang^{1,2,3,4,23}, Sethuramasundaram Pitchiaya^{1,2,23}, Marcin Cieřlik^{1,2,23}, Yashar S. Niknafs^{1,5}, Jean C.-Y. Tien^{1,2}, Yasuyuki Hosono¹, Matthew K. Iyer^{1,4}, Sahr Yazdani¹, Shruthi Subramaniam¹, Sudhanshu K. Shukla^{1,20}, Xia Jiang¹, Lisha Wang¹, Tzu-Ying Liu⁶, Michael Uhl⁷, Alexander R. Gawronski⁸, Yuanyuan Qiao^{1,2,9}, Lanbo Xiao¹, Saravana M. Dhanasekaran^{1,2}, Kristin M. Juckette¹, Lakshmi P. Kunju^{1,2,9}, Xuhong Cao^{1,10}, Utsav Patel¹¹, Mona Batish^{11,12}, Girish C. Shukla¹³, Michelle T. Paulsen^{9,14}, Mats Ljungman^{9,14}, Hui Jiang^{16,9}, Rohit Mehra^{2,9,15}, Rolf Backofen⁷, Cenk S. Sahinalp^{16,17}, Susan M. Freier¹⁸, Andrew T. Watt¹⁸, Shuling Guo¹⁸, John T. Wei¹⁵, Felix Y. Feng^{1,9,14,19,21}, Rohit Malik^{1,22,24} and Arul M. Chinnaiyan^{1,2,4,5,9,10,15,24*}

The androgen receptor (AR) plays a critical role in the development of the normal prostate as well as prostate cancer. Using an integrative transcriptomic analysis of prostate cancer cell lines and tissues, we identified ARLNC1 (AR-regulated long noncoding RNA 1) as an important long noncoding RNA that is strongly associated with AR signaling in prostate cancer progression. Not only was ARLNC1 induced by the AR protein, but ARLNC1 stabilized the AR transcript via RNA–RNA interaction. ARLNC1 knockdown suppressed AR expression, global AR signaling and prostate cancer growth in vitro and in vivo. Taken together, these data support a role for ARLNC1 in maintaining a positive feedback loop that potentiates AR signaling during prostate cancer progression and identify ARLNC1 as a novel therapeutic target.

Long noncoding RNAs (lncRNAs) are a class of transcripts with diverse and largely uncharacterized biological functions^{1–3}. Through crosstalk with chromatin, DNA, RNA species and proteins, lncRNAs function via chromatin remodeling, as well as transcriptional and post-transcriptional regulation^{4–9}. High-throughput RNA sequencing (RNA-seq) has enabled the identification of lncRNAs with suggested oncogenic and tumor-suppressive roles, including involvement in the pathogenesis of prostate cancer^{7,10–12}. Primary prostate cancer is often hormone dependent and relies on signaling through the AR; therefore, the majority of patients are responsive to front-line treatment with androgen-deprivation therapy^{13–15}. However, approximately 20% of cases progress to an incurable stage of the disease known as castration-resistant prostate cancer (CRPC), which still critically relies on AR signaling^{16,17},

as evidenced by the clinical benefit afforded through the use of enzalutamide^{18–21} or abiraterone^{22–24}. While substantial efforts have been undertaken to identify mechanisms of sustained AR signaling in CRPC (i.e., AR alterations, AR splice variants and alternative activation pathways)^{25–31}, few studies have investigated the role of AR-regulated lncRNAs. Therefore, we initiated a comprehensive RNA-seq profiling investigation of AR-regulated, cancer-associated lncRNAs from prostate cancer cell lines and patient tissue samples.

Results

Analysis of AR-regulated transcriptome in prostate cancer. To nominate AR-regulated genes (ARGs), RNA-seq was performed on AR-dependent VCaP and LNCaP prostate cancer cell lines that were stimulated with an AR ligand, dihydrotestosterone (DHT), for 6 and

¹Michigan Center for Translational Pathology, University of Michigan, Ann Arbor, MI, USA. ²Department of Pathology, University of Michigan, Ann Arbor, MI, USA. ³Molecular and Cellular Pathology Program, University of Michigan, Ann Arbor, MI, USA. ⁴Department of Computational Medicine and Bioinformatics, Ann Arbor, MI, USA. ⁵Department of Cellular and Molecular Biology, University of Michigan, Ann Arbor, MI, USA. ⁶Department of Biostatistics, University of Michigan, Ann Arbor, MI, USA. ⁷Department of Computer Science and Centre for Biological Signaling Studies (BIOSS), University of Freiburg, Freiburg, Germany. ⁸School of Computing Science, Simon Fraser University, Burnaby, British Columbia, Canada. ⁹Rogel Cancer Center, University of Michigan, Ann Arbor, MI, USA. ¹⁰Howard Hughes Medical Institute, University of Michigan, Ann Arbor, MI, USA. ¹¹New Jersey Medical School, Rutgers University, Newark, NJ, USA. ¹²Department of Medical Laboratory Sciences, University of Delaware, Newark, DE, USA. ¹³Department of Biological, Geological and Environmental Sciences, Center for Gene Regulation in Health and Disease, Cleveland State University, Cleveland, OH, USA. ¹⁴Department of Radiation Oncology, University of Michigan, Ann Arbor, MI, USA. ¹⁵Department of Urology, University of Michigan, Ann Arbor, MI, USA. ¹⁶School of Informatics and Computing, Indiana University, Bloomington, IN, USA. ¹⁷Vancouver Prostate Centre, Vancouver, British Columbia, Canada. ¹⁸Ionis Pharmaceuticals, Carlsbad, CA, USA. ¹⁹Breast Oncology Program, University of Michigan, Ann Arbor, MI, USA. Present address: ²⁰Department of Biosciences and Bioengineering, Indian Institute of Technology Dharwad, Dharwad, India. ²¹Departments of Radiation Oncology, Urology, and Medicine, Helen Diller Family Comprehensive Cancer Center, University of California at San Francisco, San Francisco, CA, USA. ²²Bristol-Myers Squibb, Princeton, NJ, USA. ²³These authors contributed equally: Yajia Zhang, Sethuramasundaram Pitchiaya, Marcin Cieřlik. ²⁴These authors jointly supervised this work: Rohit Malik, Arul M. Chinnaiyan. *e-mail: arul@umich.edu

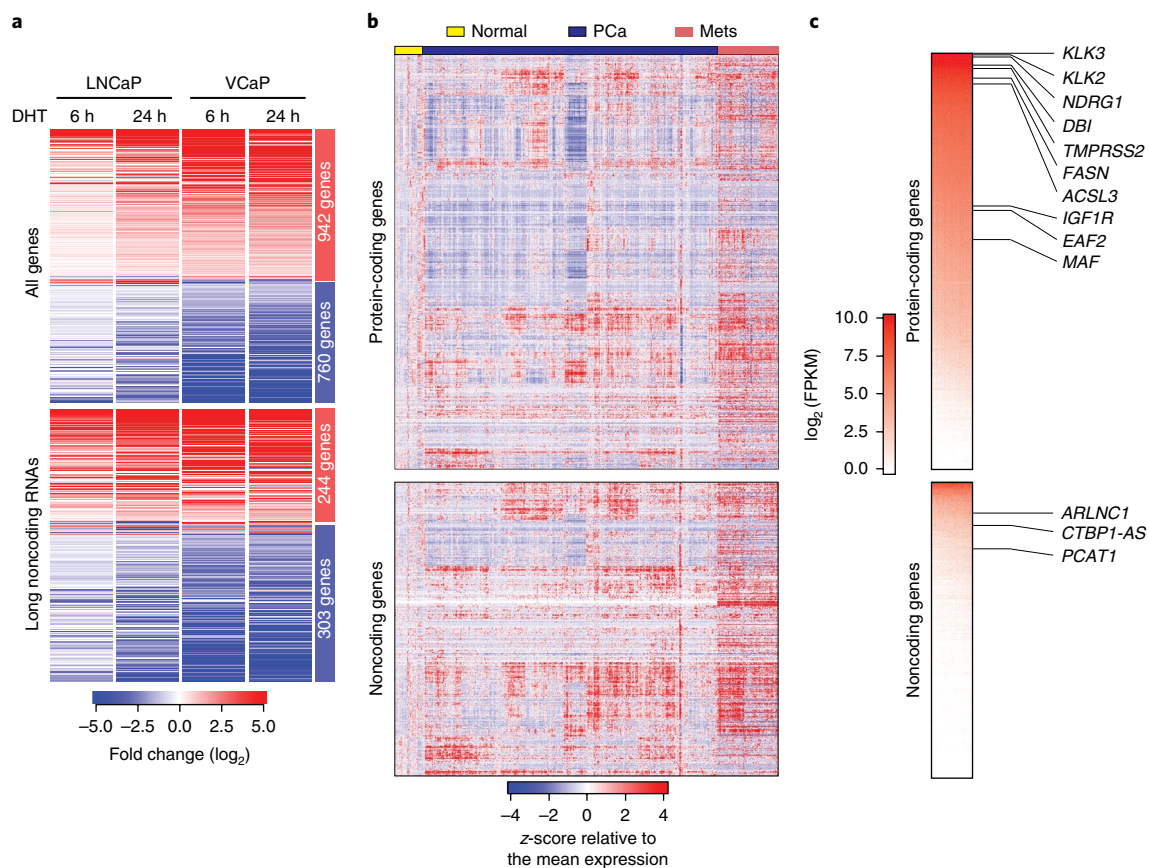


Fig. 1 | Identification of AR-regulated genes in prostate cancer. a, The androgen-regulated transcriptome of prostate cancer cells. The heat map represents the 1,702 genes (including 547 lncRNAs) differentially regulated in LNCaP and VCaP cells following 6 and 24 h of DHT treatment. **b**, The landscape of transcriptomic alterations of prostate cancer progression. The heat map depicts 1,155 protein-coding genes and 547 lncRNAs across benign prostate (normal, $n=52$ samples), localized prostate cancer (PCa, $n=500$ samples) and metastatic prostate cancer (Mets, $n=100$ samples) in TCGA prostate and SU2C-PCF RNA-seq data, with rows representing genes and columns representing patients. Patients were grouped by clinical stage, and genes were subjected to hierarchical clustering. Expression variability is quantified for each gene as a z-score relative to the mean expression in normal prostate samples. **c**, A heat map representation of ranked median gene expression levels in prostate tissues. Canonical prostate lineage and prostate cancer markers are listed.

24 h (Supplementary Fig. 1a). A total of 1,702 genes were identified to be concordantly induced or repressed in VCaP and LNCaP cells at both time points (Fig. 1a, Supplementary Fig. 1b,c and Supplementary Table 1), including more than 500 lncRNAs (Fig. 1a and Supplementary Fig. 1d); these data indicate that a large portion of the AR transcriptome remains uncharacterized.

To differentiate between direct and indirect ARGs, previously published and in-house AR chromatin immunoprecipitation (ChIP)-seq data from LNCaP and VCaP cells were analyzed³². As expected for direct AR targets, increased levels of AR binding at transcription start sites (TSSs) in both LNCaP and VCaP cells were observed (Supplementary Fig. 1e). The binding levels decreased following treatment with an AR antagonist (enzalutamide) (Supplementary Fig. 1f,g), and the binding sites revealed a de novo motif identical to the canonical AR response element³³ (Supplementary Fig. 1h). A total of 987 genes were categorized as direct ARGs, including 341 lncRNAs (lncARGs) (Supplementary Table 1). Within these genes, we observed an enrichment of chromatin marks associated with ‘open’ chromatin (H3K27ac, H3K4me1), active promoters (H3K4me3) and transcription (H3K36me3), which, together with RNA polymerase II (PolII) occupancy, are recognized as manifestations of active gene expression (Supplementary Fig. 1i). Bromodomain and extra-terminal (BET) family proteins, such as BRD4, recognize acetylated

histones and have been shown to promote AR transcriptional activity³². Consistent with this, we observed colocalization of BRD4 and AR proteins at the promoters of direct AR-responsive genes and loss of AR ChIP peaks following treatment with a bromodomain inhibitor (JQ1) (Supplementary Fig. 1f,i). We further sought to determine whether ARGs identified from cell lines were also targeted by AR in normal prostate tissues and primary tumors. We leveraged a published dataset³⁴ and queried for the presence of AR peaks within ARG promoters. Remarkably, the majority of ARG promoters were TSS-proximally bound by AR in both tissues and cell lines (Supplementary Fig. 1j,k); conversely, AR-independent genes were distal to AR-binding sites (Supplementary Fig. 1l).

Finally, we confirmed that the ARGs were also expressed in human prostate tissues. We interrogated RNA-seq data from normal prostate, clinically localized prostate cancer (The Cancer Genome Atlas, TCGA)³⁵ and metastatic CRPC (Stand Up to Cancer-Prostate Cancer Foundation, SU2C-PCF)³⁰ (Fig. 1b). This revealed remarkable heterogeneity in the expression of ARGs during prostate cancer progression to metastatic disease. As expected, compared to protein-coding genes, noncoding ARGs were detected at lower overall levels (Fig. 1c), although ~10% showed robust expression of over 10 FPKM (fragments per kilobase of transcript per million mapped reads) on average across prostate cancer samples.

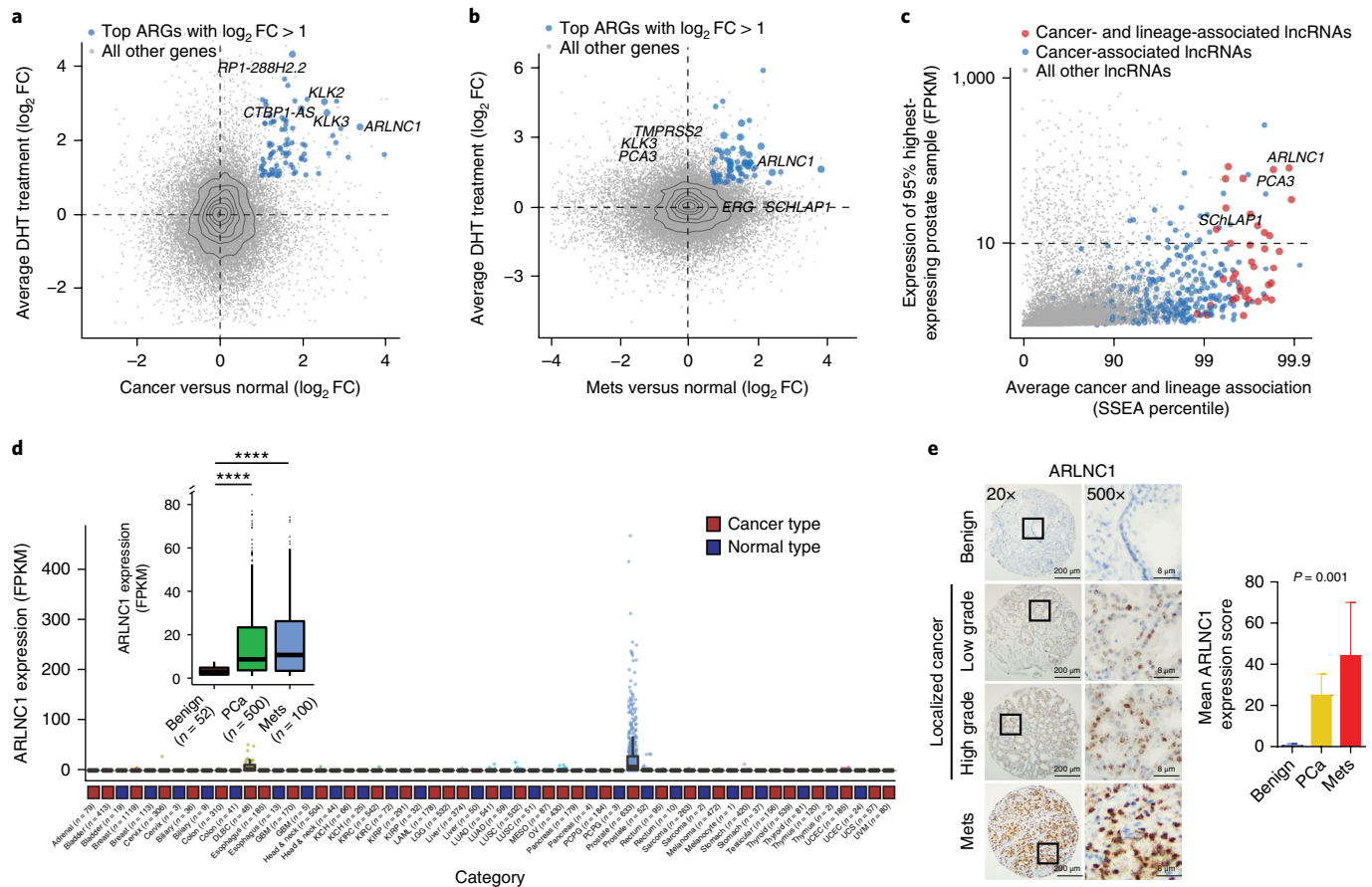


Fig. 2 | Nomination and in situ characterization of ARLNC1 in prostate cancer. **a, b**, Identification of androgen-regulated transcripts elevated in prostate cancer progression. Scatterplots show the AR regulation and cancer association of the ARGs identified in Fig. 1a. The y axis depicts the \log_2 -transformed fold change in gene expression following DHT stimulation, and the x axis indicates the \log_2 -transformed difference in gene expression level between benign prostate ($n = 52$ samples) and localized prostate cancer ($n = 500$ samples) (**a**) and between benign prostate ($n = 52$ samples) and metastatic prostate cancer ($n = 100$ samples) (**b**). Significant genes with \log_2 fold change > 1 were ranked according to combined P value (limma-moderated t test). **c**, Nomination of prostate cancer- and lineage-associated lncRNAs based on expression levels. The scatterplot shows the expression level, prostate tissue specificity and prostate cancer association of lncRNAs. The expression level is the FPKM value at the 95th percentile across TCGA prostate samples. Average cancer and lineage associations are represented by the percentile rank for each gene in SSEA (total $n = 7,256$ samples). **d**, Relative expression (FPKM) of ARLNC1 across different cancer types in the TCGA cohort. Inset, relative expression (FPKM) of ARLNC1 across benign prostate ($n = 52$ samples), localized prostate cancer ($n = 500$ samples) and metastatic prostate cancer ($n = 100$ samples). PCa versus Normal: $****P = 2.6 \times 10^{-7}$ (two-sided t test). Box-plot definitions: the center line depicts the median, the box shows the first and third quartiles, and the whiskers follow the 1.5 rule. **e**, ISH of ARLNC1 transcript in a human prostate cancer tissue microarray. Representative ARLNC1 staining is shown for benign prostate and localized and metastatic prostate cancer tissue. The bar plot represents mean ARLNC1 expression scores across benign prostate ($n = 11$), localized prostate cancer ($n = 85$) and metastatic prostate cancer ($n = 37$) tissues, with vertical bars indicating the bootstrapped 95% confidence interval of the means. Significance was calculated by a Kruskal–Wallis rank-sum test.

ARLNC1 is a prostate lineage-specific lncRNA with elevated expression in cancer. We hypothesized that lncRNAs associated with prostate cancer progression and castration resistance should be either upregulated if they enhance AR signaling or, conversely, downregulated if they attenuate AR signaling. Their expression is also expected to be AR dependent and lineage restricted if they are part of bona fide physiological feedback loops. Accordingly, a top-down strategy was developed to establish and prioritize clinically relevant, prostate cancer- and lineage-specific lncARGs. First, we identified genes that were both regulated by AR in the VCaP and LNCaP cell lines and upregulated in primary (Fig. 2a) or metastatic (Fig. 2b) prostate cancer as compared to normal prostate tissues. As expected, canonical AR targets, including *KLK3*, *KLK2* and *TMPRSS2*, were among the most differentially expressed protein-coding genes. Notably, this approach highlighted several novel lncARGs, including *ARLNC1*

(*ENSG00000260896*, *PRCAT47¹⁰*), and validated previously identified lncARGs, such as *CTBP1-AS³⁶* (Fig. 2a,b). Interestingly, *ARLNC1* was found to be one of the most differentially expressed AR-regulated genes in both localized and metastatic prostate cancer (Fig. 2a,b and Supplementary Fig. 2a,b).

Next, we sought to establish the prostate lineage and cancer specificity of prostate cancer-associated lncRNAs. We leveraged the MiTranscriptome assembly¹⁰, an online resource, to interrogate lncRNA expression across a multitude of tissue and tumor types, and we calculated sample set enrichment analysis (SSEA) scores, which indicate the strength of cancer and lineage association¹⁰. After applying an expression-level filter (10 FPKM at the 95th percentile), we identified 12 of the most prostate lineage- and cancer-specific lncRNAs (Fig. 2c and Supplementary Fig. 2c,d); 5 of these lncRNAs were regulated by AR. Across these analyses, *ARLNC1* was the top prioritized transcript and thus warranted further investigation.

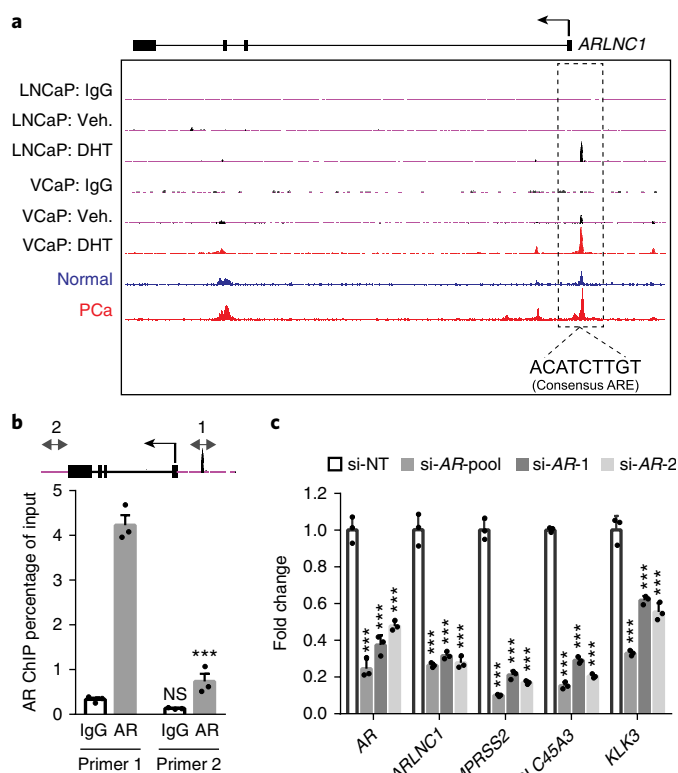


Fig. 3 | *ARLNC1* is directly regulated by AR. **a**, AR ChIP-seq in prostate cancer cell lines and tissues. Normalized ChIP-seq enrichment is shown. Top, AR or control (IgG) ChIP-seq results across the *ARLNC1* locus in LNCaP and VCaP cells with vehicle (ethanol) or DHT treatment. Bottom, AR ChIP-seq in benign prostate and clinically localized prostate cancer tissue. ARE, androgen response element. **b**, ChIP-qPCR in MDA-PCa-2b cells showing AR or IgG enrichment (ChIP/input) over the *ARLNC1* promoter region (primer 1) or a control region (primer 2). Data are shown as the mean \pm s.e.m. ($n=3$ biologically independent samples). *** P (adjusted) < 0.0001 , NS (not significant): $P=0.5746$, compared to the control region (primer 2) by ANOVA with Sidak correction for multiple comparisons. Top, schematic of the amplicon locations for ChIP-qPCR validation. **c**, Expression of *AR* and *AR* target genes (*ARLNC1*, *TMPRSS2*, *SLC45A3* and *KLK3*) in MDA-PCa-2b cells transfected with control siRNA (si-NT) or siRNAs against *AR* (si-AR-pool, si-AR-1, si-AR-2). Mean \pm s.e.m. values are shown, $n=3$ biologically independent samples. *** $P=0.0001$, determined by ANOVA with Dunnett's multiple-comparisons test.

Expression of *ARLNC1* was interrogated across cancer and normal tissue RNA-seq samples from TCGA and the Genotype-Tissue Expression (GTEx) project^{37,38}, respectively. In the TCGA cohort, *ARLNC1* exhibited a highly prostate cancer-specific expression pattern, with little to no expression in other tumor types (Fig. 2d). Similarly, in the GTEx normal tissue cohort, its expression was limited to the prostate (Supplementary Fig. 2e). Among the prostate samples, *ARLNC1* expression was significantly higher in localized and metastatic prostate cancers than in benign tissues, as assessed by RNA-seq (Fig. 2d, inset) and in situ hybridization (ISH; Fig. 2e). In an extensive differential expression analysis using MiTranscriptome, *ARLNC1* was found to be among the top 1% of transcripts most upregulated in prostate cancer and specific to the prostate lineage, with no significant associations in other tissues (Supplementary Fig. 2f). Moreover, the protein-coding genes that were most correlated with *ARLNC1* were found to be associated with prostate cancer progression in ONCOMINE concept analyses performed on multiple clinical datasets³⁹ (Supplementary Fig. 2g). Together, these

results confirm that *ARLNC1* expression is restricted to the prostate lineage, elevated in prostate cancer and associated with AR signaling throughout prostate cancer progression.

To functionally characterize *ARLNC1*, we first identified appropriate prostate cancer cell lines with moderate to high levels of *ARLNC1* expression using in-house RNA-seq data (Supplementary Fig. 3a). Supporting the association of AR with *ARLNC1*, *ARLNC1* expression was highly enriched in AR-positive cell lines, with the highest expression in MDA-PCa-2b and LNCaP cells. In addition, qPCR analysis for the *ARLNC1* transcript also demonstrated that this gene was expressed at the highest level in the MDA-PCa-2b and LNCaP cell lines (Supplementary Fig. 3b). As existing annotations of the *ARLNC1* gene (located on chromosome 16) predict the presence of several transcript isoforms that differ in exon and TSS usage, we determined the exact structure in MDA-PCa-2b and LNCaP cells by RACE. A common TSS for *ARLNC1* was found in both cell lines, and the ~2.8-kb transcript isoform was further confirmed by northern blot analysis (Supplementary Fig. 3c). Single-molecule FISH (smFISH) revealed that approximately 100 molecules of *ARLNC1* transcript existed per MDA-PCa-2b cell (Supplementary Fig. 3d,e). Using smFISH and qPCR, we also found that *ARLNC1* molecules were distributed equally between the nuclear and cytoplasmic cellular compartments (Supplementary Fig. 3f,g).

***ARLNC1* transcription is directly regulated by AR.** Because *ARLNC1* was identified as an AR-regulated lncRNA, we inspected the promoter region of the *ARLNC1* gene for AR occupancy and identified an androgen-induced AR peak in AR ChIP-seq data from both DHT-stimulated VCaP and LNCaP cells (Fig. 3a). Notably, this AR-binding site was also observed in prostate tissue samples and contained a canonical androgen response element³³ (Fig. 3a). These observations were corroborated by ChIP-qPCR in MDA-PCa-2b cells, which showed the highest level of *ARLNC1* expression (Fig. 3b). Considering the observation that *ARLNC1* expression is prostate tissue specific, while AR expression is not as much, we searched for additional regulators (transcription factors and epigenetic modifiers) of the *ARLNC1* gene (Supplementary Fig. 4a). Motif analysis of the *ARLNC1* promoter region identified several transcription factor binding sites, including a FOXA1 response element. To further validate *ARLNC1* gene regulation by AR and FOXA1, we evaluated *ARLNC1* transcript levels following AR or FOXA1 knockdown. AR or FOXA1 loss resulted in decreased expression of *ARLNC1*, along with other canonical AR target genes that served as positive controls (Fig. 3c and Supplementary Fig. 4b). ChIP-seq and ChIP-qPCR analyses additionally confirmed the putative FOXA1-binding motif on the *ARLNC1* promoter (Supplementary Fig. 4c). Together, these observations suggest that *ARLNC1* is directly regulated by AR and modestly regulated by FOXA1, which partially explains the tissue-specific expression pattern of *ARLNC1*, as expression of these two transcription factors overlaps nearly exclusively in prostate tissue^{37,38} (Supplementary Fig. 4d).

***ARLNC1* regulates AR signaling.** To elucidate the function of *ARLNC1* in prostate cancer, we performed gene expression profiling of wild-type and *ARLNC1*-knockdown MDA-PCa-2b cells (Fig. 4a). Gene ontology (GO) pathway enrichment analysis of the differentially expressed genes revealed deregulation of four main biological activities: apoptosis, cell proliferation, DNA damage response and androgen signaling (Fig. 4a). The significant decrease in AR target gene expression is particularly interesting given the fact that *ARLNC1* is regulated by AR, suggesting a positive feedback loop between *ARLNC1* and AR signaling. To confirm this observation, we generated an AR target gene signature from MDA-PCa-2b cells stimulated with DHT (Supplementary Fig. 5a and Supplementary Table 2) and performed gene set enrichment analysis (GSEA) using this gene signature (Fig. 4b). Knockdown

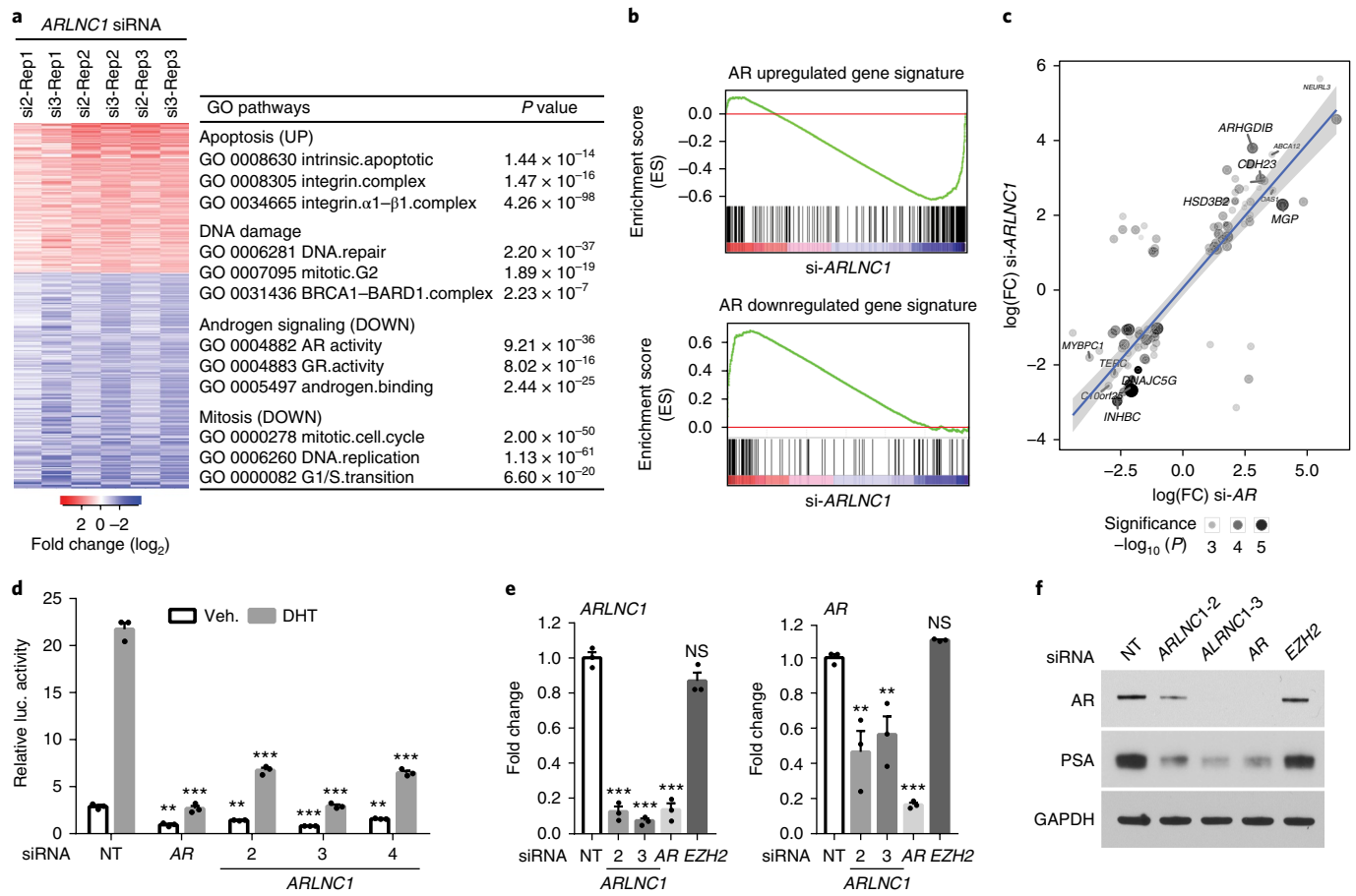


Fig. 4 | *ARLNC1* loss attenuates AR signaling. **a**, Gene expression profiling for *ARLNC1* knockdown in MDA-PCa-2b cells ($n=3$ biologically independent cell cultures for each siRNA). The chart presents the top enriched pathways following *ARLNC1* knockdown, identified using GO enrichment analysis (RandomSet test). **b**, GSEA showing significant enrichment of the *ARLNC1*-regulated gene set with respect to the AR target gene sets ($n=3$ independent gene expression profiles). Shown are enrichment plots for gene sets consisting of genes positively regulated by AR (top) and genes negatively regulated by AR (bottom). **c**, Comparison of *ARLNC1*-regulated and AR target genes based on RNA-seq following knockdown of AR and *ARLNC1*. Significant genes and their log-transformed fold changes in either of the conditions are shown ($n=2$ independent cell cultures per-condition). Combined significance levels, determined by a limma-moderated t test (across both knockdowns), are indicated by circle size. **d**, siRNA knockdown of *ARLNC1* in MDA-PCa-2b cells impairs AR signaling as determined by AR reporter gene assay. siRNA against *AR* serves as a positive control for inhibition of AR signaling. Mean \pm s.e.m. values are shown, $n=3$ biologically independent cell cultures. $**P<0.01$, $***P=0.0001$, determined by ANOVA with Dunnett correction. **e**, qRT-PCR analysis of *ARLNC1* and *AR* in MDA-PCa-2b cells transfected with siRNAs against *ARLNC1*, *AR*, *EZH2* or non-specific control (NT). siRNA against *AR* serves as a positive control for inhibition of AR signaling, while siRNA against *EZH2* serves as a negative control. Mean \pm s.e.m. values are shown, $n=3$. $**P<0.01$, $***P=0.0001$, determined by ANOVA with Dunnett correction. **f**, Immunoblots of AR, PSA and GAPDH in MDA-PCa-2b cells transfected with siRNAs against *ARLNC1*, *AR*, *EZH2* or non-specific control (NT). The experiments were repeated three times independently with similar results. Uncropped images are shown in Supplementary Fig. 9.

of *ARLNC1* led to suppression of genes positively regulated by AR and upregulation of genes negatively regulated by AR (Fig. 4b,c and Supplementary Fig. 5b). This was further confirmed by an AR reporter activity assay (Fig. 4d and Supplementary Fig. 5c), as well as qPCR analysis of AR target genes (Supplementary Fig. 5d). Interestingly, *ARLNC1* knockdown also had a significant effect on the mRNA and protein levels of AR (Fig. 4e,f), suggesting direct regulation of AR by *ARLNC1*. However, we found that *ARLNC1* overexpression did not affect AR and its signaling cascade (Supplementary Fig. 5e).

In situ colocalization of *ARLNC1* and *AR* transcripts. Noncoding RNAs have been shown to target mRNAs via direct or indirect RNA-RNA interaction^{9,40-42}. To identify target mRNAs that could interact with *ARLNC1*, we performed unbiased prediction of RNA-RNA interactions using IntraRNA^{43,44}. Interestingly, the 3' UTR of the *AR* transcript was identified as a target of *ARLNC1*

(Fig. 5a and Supplementary Fig. 6a). An in vitro RNA-RNA interaction assay between the 3' UTR of *AR* and full-length *ARLNC1* confirmed this in silico prediction (Fig. 5b). To evaluate this interaction in the context of the cellular environment, multiplexed smFISH for *AR* and *ARLNC1* transcripts was performed in MDA-PCa-2b cells. On co-staining of MDA-PCa-2b cells for either a combination of *AR* transcripts and a panel of lncRNAs or *ARLNC1* and a panel of mRNAs, we observed specific colocalization of *AR* and *ARLNC1* transcripts in the nucleus within foci that were typically larger than individual molecules (Fig. 5c-e). The extent of colocalization was much higher than that expected from coincidental colocalization with an abundant transcript, such as MALAT1 or *GAPDH* (Fig. 5c-e). More specifically, colocalization typically occurred at a stoichiometry of 2:1 *ARLNC1/AR*, which accounted for ~10-20% of all *AR* and *ARLNC1* transcripts in the cell (Supplementary Fig. 6b). Furthermore, *AR-ARLNC1* colocalization was observed in *ARLNC1*-positive prostate cancer tissues (Fig. 5f,g).

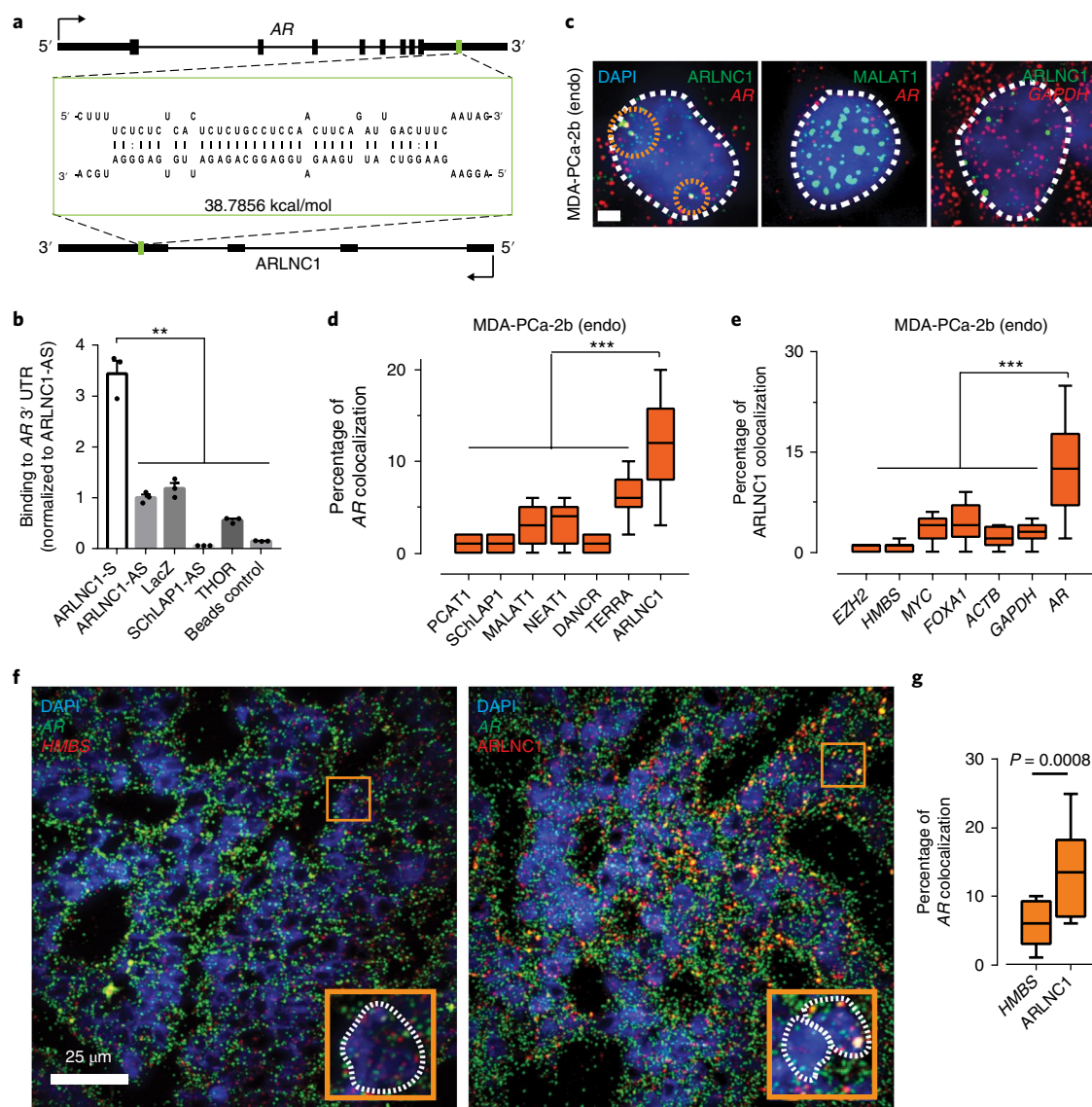


Fig. 5 | In situ colocalization of AR mRNA and ARLNC1 in prostate cancer cells. **a**, Schematic of the predicted RNA-RNA interaction between ARLNC1 and the 3' UTR of AR. **b**, ARLNC1 interacts with the AR 3' UTR in an in vitro RNA-RNA interaction assay. Compared to a panel of control RNAs (ARLNC1 antisense, LacZ, SCHLAP1-AS, THOR), ARLNC1 binds to AR 3' UTR-1-980 with high affinity. The binding affinity was quantified by qPCR analysis of the AR 3' UTR. Data were normalized to the ARLNC1-AS control. Mean \pm s.e.m. are shown, $n=3$. $**P < 0.001$, by two-tailed Student's t test. **c-e**, smFISH depiction of AR-ARLNC1 colocalization in situ. **c**, Representative pseudocolored images of MDA-PCa-2b cell nuclei stained for the appropriate endogenous (endo) transcripts (green, red) and with DAPI (nucleus, blue). Scale bar, 5 μ m. The orange circles represent regions of colocalization. **d,e**, Quantification of the percentage of AR or ARLNC1 molecules colocalizing with a panel of lncRNAs (**d**) or mRNAs (**e**). The center line and whiskers depict the median and range, respectively, and the box extends from the 25th to the 75th percentile ($n=50$ cells for each sample aggregated from 3 independent experiments). $***P < 0.0001$, by two-tailed Student's t test. **f**, Representative pseudocolored images of ARLNC1-positive prostate cancer tissues stained with DAPI (nucleus, blue) and for AR (green), HMBS (red) or ARLNC1 (red) transcripts (smFISH). Inset, $5.5 \times 5.5 \mu\text{m}^2$ zoomed-in view of the box within the main panel. **g**, Quantification of the percentage of AR molecules colocalizing with HMBS transcripts or ARLNC1. The center line and whiskers depict the median and range, respectively, and the box extends from the 25th to the 75th percentile ($n=15$ field-of-views for each sample aggregated from 3 independent tissues). $P < 0.001$, by two-tailed Student's t test.

Using an in vitro RNA-RNA binding assay, we identified nucleotides 700–1300 of ARLNC1 to be critical for binding to the AR 3' UTR (Fig. 6a,b). To confirm this observation within the cellular context, we ectopically overexpressed different fragments of ARLNC1 together with AR in U2OS osteosarcoma cells. In this exogenous system, colocalization of AR and ARLNC1 was once again demonstrated, wherein colocalization was dependent on the presence of nucleotides 700–1300 of ARLNC1 (Fig. 6c,d and Supplementary Fig. 6c). Furthermore, incubation with antisense oligonucleotides (ASOs) that blocked the interaction site led to a

significant reduction in ARLNC1-AR interaction in vitro and in situ (Fig. 6e,f and Supplementary Fig. 6d,e). Decreased AR signaling was also observed following blocking of this interaction (Fig. 6g and Supplementary Fig. 6f).

ARLNC1 regulates the cytoplasmic levels of AR transcripts. We then sought to delineate the mechanism of ARLNC1-mediated AR regulation. We first monitored the stability of these two transcripts and found that AR and ARLNC1 have similar half-lives of ~ 9 h (Supplementary Fig. 6g). As ARLNC1 depletion resulted in a

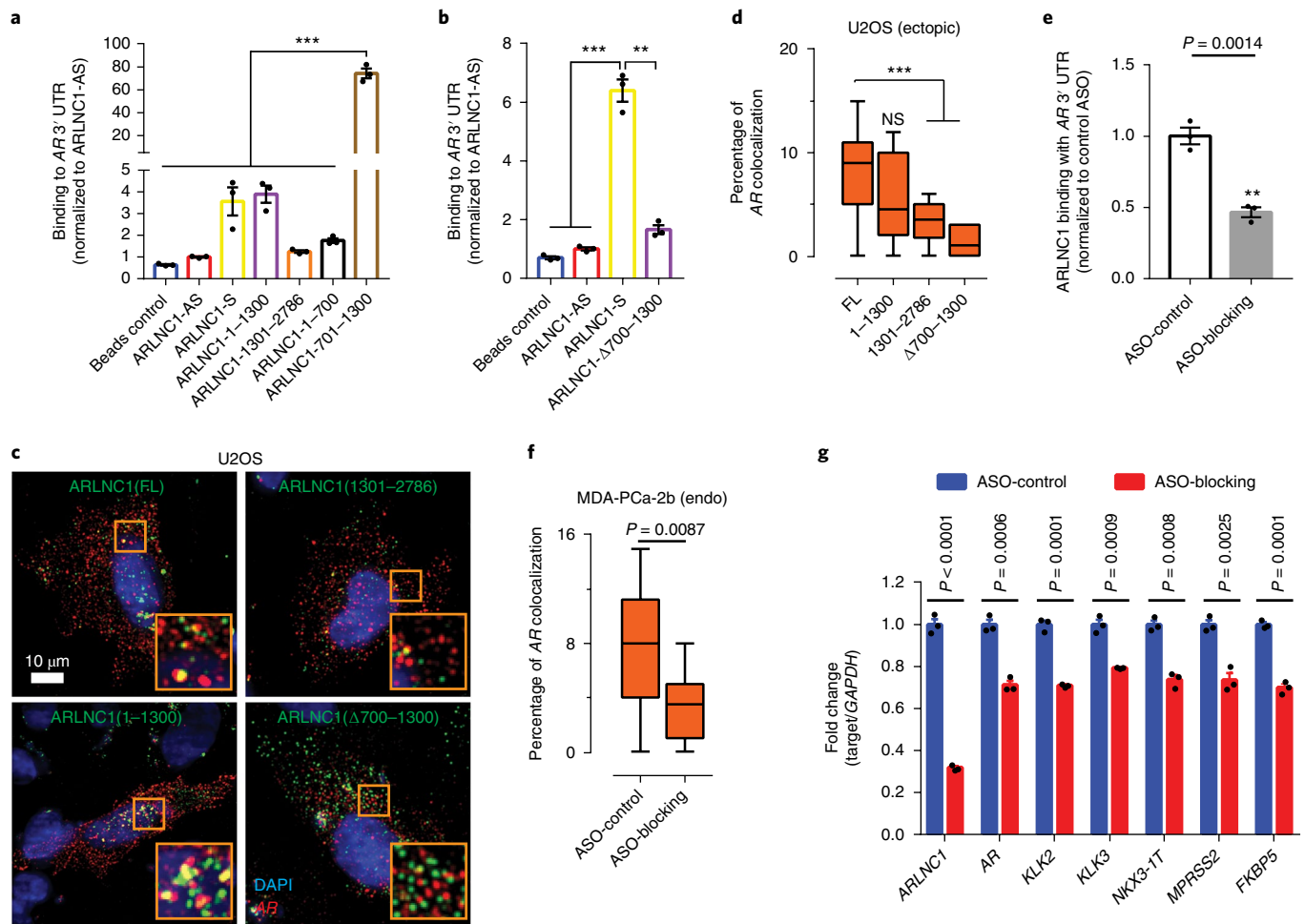


Fig. 6 | Identification of the ARLNC1 fragment mediating RNA-RNA interaction with AR mRNA. **a**, In vitro RNA-RNA interaction assay identifies nucleotides 700–1300 on ARLNC1 as critical binding site to AR 3' UTR-1–980. ARLNC1 fragments covering nucleotides 700–1300 display comparable or higher AR 3' UTR binding affinity than ARLNC1-S, with ARLNC1-700–1300 exhibiting the highest binding affinity. Data were normalized to the ARLNC1-AS control. Mean \pm s.e.m. values are shown, $n=3$. $***P$ (adjusted) = 0.0001, determined by ANOVA with Dunnett's multiple-comparisons test. **b**, Deletion of nucleotides 700–1300 on ARLNC1 results in impaired binding to the AR 3' UTR, as shown by in vitro RNA-RNA interaction assay. Data were normalized to the ARLNC1-AS control. Mean \pm s.e.m. values are shown, $n=3$. $***P=0.0001$, $**P=0.0003$, by two-tailed Student's t test. **c,d**, smFISH shows that nucleotides 700–1300 in ARLNC1 are important for colocalization in situ. **c**, Representative pseudocolored images of U2OS cells stained with DAPI (nucleus, blue) and for ARLNC1 (green) and AR transcripts (red). Inset, $10 \times 10 \mu\text{m}^2$ zoomed-in view of the orange box in the main image. **d**, Quantification of the percentage of AR molecules colocalizing with various ARLNC1 fragments. The center line and whiskers depict the median and range, respectively, and the box extends from the 25th to the 75th percentile ($n=50$ cells for each sample aggregated from 3 independent experiments). $***P < 0.0001$, by two-tailed Student's t test. NS, not significant. **e**, ASOs targeting nucleotides 700–1300 on the ARLNC1 transcript (ASO-blocking pool) inhibit ARLNC1 interaction with the AR 3' UTR. In vitro RNA-RNA interaction assays were performed using ARLNC1 and the AR 3' UTR, with the addition of the blocking ASO pool or control ASO. Data were normalized to the control ASO. Mean \pm s.e.m. values are shown, $n=3$. $P=0.0014$, by two-tailed Student's t test. **f**, smFISH shows that ASOs targeting nucleotides 700–1300 on the ARLNC1 transcript (ASO-blocking) inhibit ARLNC1 colocalization with AR in situ. Quantification is shown of the percentage of AR transcripts colocalizing with ARLNC1 after various treatments in MDA-PCa-2b cells. The center line and whiskers depict the median and range, respectively, and the box extends from the 25th to the 75th percentile ($n=50$ cells for each sample aggregated from 3 independent experiments). The P value was computed by two-tailed Student's t test. **g**, qPCR analysis of *ARLNC1*, *AR* and AR signaling genes (*KLK2*, *KLK3*, *NKX3-1*, *TMPRSS2* and *FKBP5*) in MDA-PCa-2b cells transfected with control or blocking ASOs targeting the interaction site between ARLNC1 and the AR 3' UTR. Mean \pm s.e.m. values are shown, $n=3$. Significance was determined by two-tailed Student's t test.

striking reduction of AR protein levels, much more than could be explained by AR transcript reduction, we hypothesized that ARLNC1 could affect AR post-transcriptionally. To test this hypothesis, we tracked the subcellular localization of AR transcripts using smFISH after depleting ARLNC1. We confirmed successful in situ knockdown of ARLNC1 using siRNAs, antisense oligonucleotide (ASO) and the blocking oligonucleotides that targeted the ARLNC1–AR interaction (ASO-blocking) in MDA-PCa-2b cells (Supplementary Fig. 6h,i). Quantification of the subcellular distribution of ARLNC1

suggested that the nuclear fraction of ARLNC1 was enriched only in the ARLNC1 siRNA (si-ARLNC1) condition (Supplementary Fig. 6j), a result expected for siRNAs that are typically more functional in the cytosol⁴⁵. Surprisingly, ARLNC1 knockdown or obstruction of the AR–ARLNC1 interaction increased the nuclear AR fraction by dramatically decreasing cytoplasmic levels of the AR transcript (Fig. 7a,b and Supplementary Fig. 6k–l). This observation was further supported by BrU-seq and BrUChase-seq, two high-throughput tools that monitor transcript synthesis and stability. On ARLNC1

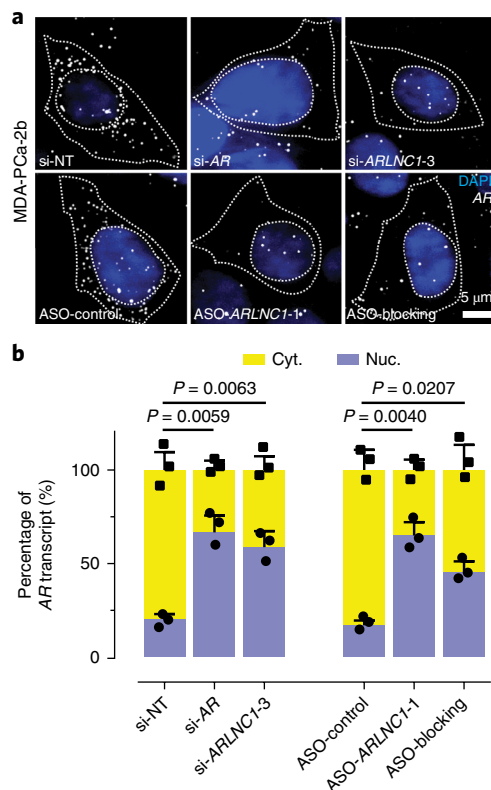


Fig. 7 | ARLNC1 regulates the cytoplasmic level of the AR transcript.

a, ARLNC1 regulates AR post-transcriptionally by specifically affecting cytoplasmic AR mRNA. Representative pseudocolored images are shown of MDA-PCa-2b cells stained for DAPI (nucleus, blue) and AR (gray) after treatment with siRNA against AR (si-AR), siRNA against ARLNC1 (si-ARLNC1-3), ASO against ARLNC1 (ASO-ARLNC1-1) or blocking ASO against the AR-ARLNC1 colocalizing segment (ASO-blocking). Quantification of knockdown is shown in Supplementary Fig. 6k,l. **b**, Fractional column plots depicting the nucleo-cytoplasmic distribution of AR mRNA after the various treatment conditions in **a**, as computed using smFISH. Mean \pm s.e.m. values are shown, $n = 3$ independent experiments and 60 cells analyzed for each sample. The P values were computed by comparing to si-NT- or ASO-control-treated cells, by two-tailed Student's t test.

knockdown, the synthesis rate of the AR transcript remained the same (Supplementary Fig. 6m), while the stability of the transcript decreased, particularly through the 3' UTR (Supplementary Fig. 6n). Taken together, our data suggest that ARLNC1 regulates the cytoplasmic levels of AR transcripts. Furthermore, the transcriptional coupling between AR and ARLNC1 transcripts is mediated by direct interactions that are encoded in their sequences.

Inhibition of ARLNC1 delays prostate cancer growth in vitro and in vivo. Having established a role for ARLNC1 in the regulation of AR signaling, we further evaluated the biological effects of ARLNC1 in prostate cancer cell lines. GO pathway enrichment analysis of the knockdown microarray data showed that ARLNC1-regulated genes were involved in cell proliferation and apoptosis (Fig. 4a). Knockdown of ARLNC1 had a significant effect on the proliferation of AR-dependent MDA-PCa-2b and LNCaP cells, but had no effect on AR-negative DU145 and PC3 cells (Fig. 8a and Supplementary Fig. 7a,b). Knockdown of ARLNC1 also resulted in increased apoptosis in AR-positive prostate cancer cells (Fig. 8b and Supplementary Fig. 7c). Notably, these results translated to effects in vivo, as cells expressing shRNA targeting ARLNC1 formed smaller tumors in mice when compared to cells expressing non-targeting

shRNA (Fig. 8c), thus suggesting that ARLNC1 is an important survival factor for AR-dependent prostate cancer.

Because modulation of ARLNC1 expression levels resulted in a striking proliferation phenotype, we hypothesized that ARLNC1 inhibition could be used therapeutically for the treatment of prostate cancer. ASOs have recently been shown to be effective in targeting RNA in vivo^{46–49}; thus, we designed ASOs targeting the ARLNC1 transcript (Supplementary Fig. 7d). Transfection of ASOs resulted in strong knockdown efficiency (Supplementary Fig. 7e), and ASO-mediated knockdown resulted in similar effects on gene expression profiling to siRNA (Fig. 8d,e and Supplementary Fig. 7f). Furthermore, AR-positive cells transfected with ARLNC1 ASOs exhibited retarded growth, similar to those treated with siRNAs (Fig. 8f). To evaluate the therapeutic potential of ARLNC1 ASOs in vivo, we first assessed the cellular free-uptake efficiency of ARLNC1 ASOs, a prerequisite for ASO therapeutic use. Notably, several ASOs significantly reduced ARLNC1 levels through free uptake (Supplementary Fig. 7g). Free uptake of ARLNC1 ASOs led to a significant decrease in the proliferation capacity of MDA-PCa-2b cells in both normal cell culture and 3D sphere conditions (Supplementary Fig. 7h–j). Treatment of mice bearing MDA-PCa-2b xenografts with ARLNC1-targeting ASOs led to significant decreases in tumor growth compared to control ASO (Fig. 8g,h and Supplementary Fig. 8a–e). Taken together, these data, along with the association of ARLNC1 with aggressive androgen signaling (Supplementary Fig. 8f–j), suggest that ARLNC1 plays a critical role in the proliferation of AR-dependent prostate cancer and can be effectively exploited as a therapeutic target.

Discussion

As AR signaling remains a significant driver of CRPC pathogenesis, it is imperative to generate novel strategies to target this pathway. Even with the addition of enzalutamide or abiraterone to CRPC treatment regimens, progression invariably occurs. Exploiting players other than AR itself that are pivotal to maintaining the magnitude of the androgen response is an alternative approach. Our comprehensive profiling of AR-regulated, prostate cancer-associated lncRNAs identified the top-ranking candidate ARLNC1 that we functionally characterized. We identified a positive feedback loop between ARLNC1 and AR that maintains the androgen transcriptional program in AR-positive prostate cancer cells, specifically through regulating the cellular levels of AR (Fig. 8i). The mechanism we identified echoes previous studies on lncRNAs—1/2-sbsRNAs⁴², BACE1-AS⁹ and TINCR⁴¹, which highlights the role of lncRNA in increasing or decreasing RNA stability.

As a novel noncoding regulator of AR signaling, ARLNC1 has the potential to be not only a mechanistic biomarker but also a therapeutic target for advanced prostate cancer. In addition, the fact that it acts upstream of AR signaling presents the possibility that targeting ARLNC1 may afford an additional option to patients that have de novo or acquired resistance to therapies targeting AR itself (that is, enzalutamide or abiraterone). Furthermore, specific antisense nucleotides targeting ARLNC1, which we demonstrate to be specifically expressed in the prostate, could circumvent undesirable side effects that occur in other tissues with exposure to androgen synthesis inhibitors or anti-androgens.

Although we have identified a new node of the AR signaling network that can be therapeutically targeted, the molecular mechanism through which ARLNC1 regulates AR transcript levels remains to be fully characterized. At this time, it is unclear whether the physical interaction between the AR 3' UTR and ARLNC1 functions with the aid of additional RNA-binding proteins (for example, HuR) and/or RNAs in vivo^{50,51}. Nonetheless, the application of ASOs has ushered in an exciting era that makes it possible to target previously 'undruggable' molecules directly at the transcript level, such as ARLNC1, which is likely to yield promising opportunities in cancer treatment.

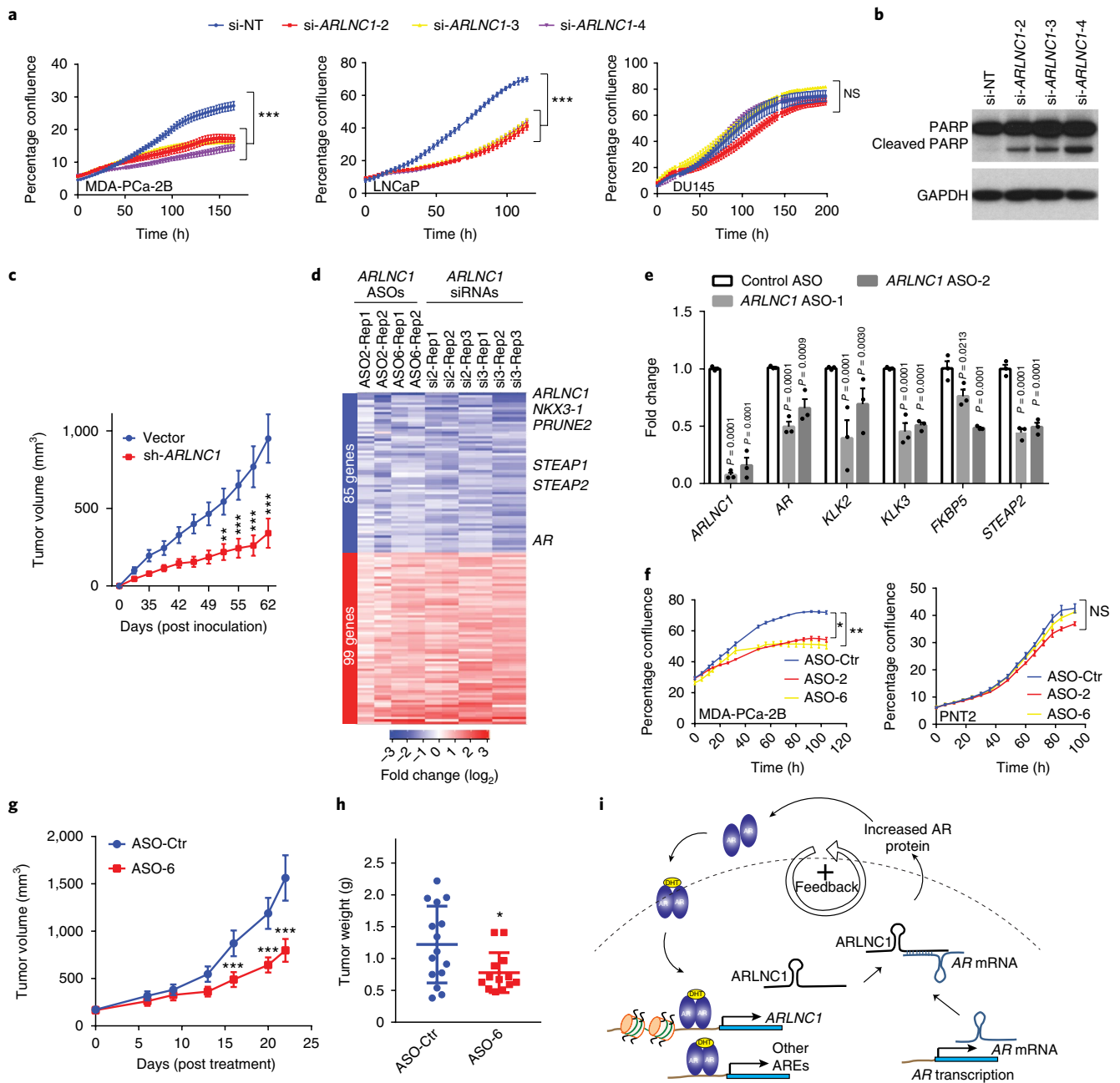


Fig. 8 | ARLNC1 as a therapeutic target in AR-positive prostate cancer models. a, siRNA-mediated knockdown of ARLNC1 in vitro in AR-positive prostate cancer cell lines (MDA-PCa-2b and LNCaP) inhibits cell proliferation. The AR-negative prostate cell line DU145 serves as a negative control. Mean \pm s.d. values are shown, $n = 6$ independent cell cultures per group, $^{**}P$ (adjusted) = 0.0001 compared to si-NT-treated cells, by one-way ANOVA with Dunnett's multiple-comparisons test; NS, not significant. **b**, ARLNC1 loss leads to increased apoptosis as shown by western blot analysis of PARP and cleaved PARP in LNCaP cells following ARLNC1 knockdown. The experiment was repeated independently three times with similar results. Uncropped images are shown in Supplementary Fig. 9. **c**, Tumor growth of LNCaP-AR cells expressing shRNA targeting ARLNC1 or shRNA vector. Mean \pm s.e.m. values are shown. $n = 10$ independent tumors, $^{***}P < 0.0001$, $^{**}P = 0.0007$, as determined by two-tailed Student's t test. **d**, Gene expression profiling for siRNA-mediated or ASO-mediated ARLNC1 knockdown in MDA-PCa-2b cells. The numbers above the heat map represent the specific microarray replicates. **e**, qRT-PCR analysis of ARLNC1, AR and AR targets (KLK2, KLK3, FKBP5 and STEAP2) in MDA-PCa-2b cells transfected with ASOs against ARLNC1. Data were normalized to a housekeeping gene, and the levels in control ASO-treated cells were set to 1. Mean \pm s.e.m. values are shown, $n = 3$. Adjusted P values were determined by one-way ANOVA with Dunnett correction for multiple comparisons. **f**, Transfection of ASOs targeting ARLNC1 in AR-positive MDA-PCa-2b cells inhibits cell proliferation. The AR-negative prostate cell line PNT2 serves as a negative control. Mean \pm s.e.m. values are shown, $n = 6$ independent cell cultures per treatment group. $^{*}P$ (adjusted) = 0.0112, $^{***}P$ (adjusted) = 0.0065, NS: not significant; compared to the control-ASO group by one-way ANOVA with Dunnett correction for multiple comparisons. **g, h**, Effect of ASO treatment on the growth of MDA-PCa-2b xenografts in male athymic nude mice, with control ASO ($n = 15$) or ARLNC1 ASO ($n = 13$) treatment subcutaneously at 50 mg per kg body weight, five times per week for 3 weeks. Tumors were measured by caliper biweekly (**g**) and tumor weights were measured at the end point (**h**). Mean \pm s.d. values are shown. $^{*}P = 0.0251$, $^{***}P < 0.0001$; compared to control ASO by two-tailed Student's t test. **i**, A model depicting the positive feedback loop between ARLNC1 and AR that is critical for prostate cancer growth.

Methods

Methods, including statements of data availability and any associated accession codes and references, are available at <https://doi.org/10.1038/s41588-018-0120-1>.

Received: 7 February 2017; Accepted: 23 March 2018;
Published online: 28 May 2018

References

1. Mercer, T. R., Dinger, M. E. & Mattick, J. S. Long non-coding RNAs: insights into functions. *Nat. Rev. Genet.* **10**, 155–159 (2009).
2. Wang, K. C. & Chang, H. Y. Molecular mechanisms of long noncoding RNAs. *Mol. Cell* **43**, 904–914 (2011).
3. Rinn, J. L. & Chang, H. Y. Genome regulation by long noncoding RNAs. *Annu. Rev. Biochem.* **81**, 145–166 (2012).
4. Rinn, J. L. et al. Functional demarcation of active and silent chromatin domains in human HOX loci by noncoding RNAs. *Cell* **129**, 1311–1323 (2007).
5. Lee, N., Moss, W. N., Yario, T. A. & Steitz, J. A. EBV noncoding RNA binds nascent RNA to drive host PAX5 to viral DNA. *Cell* **160**, 607–618 (2015).
6. Wutz, A., Rasmussen, T. P. & Jaenisch, R. Chromosomal silencing and localization are mediated by different domains of Xist RNA. *Nat. Genet.* **30**, 167–174 (2002).
7. Prensner, J. R. et al. The long noncoding RNA SchLAP1 promotes aggressive prostate cancer and antagonizes the SWI/SNF complex. *Nat. Genet.* **45**, 1392–1398 (2013).
8. Gupta, R. A. et al. Long non-coding RNA HOTAIR reprograms chromatin state to promote cancer metastasis. *Nature* **464**, 1071–1076 (2010).
9. Faghihi, M. A. et al. Expression of a noncoding RNA is elevated in Alzheimer's disease and drives rapid feed-forward regulation of β -secretase. *Nat. Med.* **14**, 723–730 (2008).
10. Iyer, M. K. et al. The landscape of long noncoding RNAs in the human transcriptome. *Nat. Genet.* **47**, 199–208 (2015).
11. Malik, R. et al. The lncRNA PCAT29 inhibits oncogenic phenotypes in prostate cancer. *Mol. Cancer Res.* **12**, 1081–1087 (2014).
12. Shukla, S. et al. Identification and validation of PCAT14 as prognostic biomarker in prostate cancer. *Neoplasia* **18**, 489–499 (2016).
13. Lu-Yao, G. L. et al. Fifteen-year survival outcomes following primary androgen-deprivation therapy for localized prostate cancer. *JAMA Intern. Med.* **174**, 1460–1467 (2014).
14. Huggins, C. & Hodges, C. V. Studies on prostatic cancer. I. The effect of castration, of estrogen and of androgen injection on serum phosphatases in metastatic carcinoma of the prostate. 1941. *J. Urol.* **167**, 948–951 (2002).
15. The Veterans Administration Co-operative Urological Research Group. Treatment and survival of patients with cancer of the prostate. *Surg. Gynecol. Obstet.* **124**, 1011–1017 (1967).
16. Chen, Y., Sawyers, C. L. & Scher, H. I. Targeting the androgen receptor pathway in prostate cancer. *Curr. Opin. Pharmacol.* **8**, 440–448 (2008).
17. Wong, Y. N., Ferraldeschi, R., Attard, G. & de Bono, J. Evolution of androgen receptor targeted therapy for advanced prostate cancer. *Nat. Rev. Clin. Oncol.* **11**, 365–376 (2014).
18. Mukherji, D., Pezaro, C. J. & De-Bono, J. S. MDV3100 for the treatment of prostate cancer. *Expert Opin. Investig. Drugs* **21**, 227–233 (2012).
19. Scher, H. I. et al. Increased survival with enzalutamide in prostate cancer after chemotherapy. *N. Engl. J. Med.* **367**, 1187–1197 (2012).
20. Tran, C. et al. Development of a second-generation antiandrogen for treatment of advanced prostate cancer. *Science* **324**, 787–790 (2009).
21. Scher, H. I. et al. Antitumor activity of MDV3100 in castration-resistant prostate cancer: a phase 1-2 study. *Lancet* **375**, 1437–1446 (2010).
22. Stein, M. N., Goodin, S. & Dipaola, R. S. Abiraterone in prostate cancer: a new angle to an old problem. *Clin. Cancer Res.* **18**, 1848–1854 (2012).
23. Reid, A. H. et al. Significant and sustained antitumor activity in post-docetaxel, castration-resistant prostate cancer with the CYP17 inhibitor abiraterone acetate. *J. Clin. Oncol.* **28**, 1489–1495 (2010).
24. de Bono, J. S. et al. Abiraterone and increased survival in metastatic prostate cancer. *N. Engl. J. Med.* **364**, 1995–2005 (2011).
25. Watson, P. A., Arora, V. K. & Sawyers, C. L. Emerging mechanisms of resistance to androgen receptor inhibitors in prostate cancer. *Nat. Rev. Cancer* **15**, 701–711 (2015).
26. Antonarakis, E. S. et al. AR-V7 and resistance to enzalutamide and abiraterone in prostate cancer. *N. Engl. J. Med.* **371**, 1028–1038 (2014).
27. Attard, G., Richards, J. & de Bono, J. S. New strategies in metastatic prostate cancer: targeting the androgen receptor signaling pathway. *Clin. Cancer Res.* **17**, 1649–1657 (2011).
28. Hearn, J. W. et al. HSD3B1 and resistance to androgen-deprivation therapy in prostate cancer: a retrospective, multicohort study. *Lancet Oncol.* **17**, 1435–1444 (2016).
29. Chan, S. C., Li, Y. & Dehm, S. M. Androgen receptor splice variants activate androgen receptor target genes and support aberrant prostate cancer cell growth independent of canonical androgen receptor nuclear localization signal. *J. Biol. Chem.* **287**, 19736–19749 (2012).
30. Robinson, D. et al. Integrative clinical genomics of advanced prostate cancer. *Cell* **161**, 1215–1228 (2015).
31. Visakorpi, T. et al. In vivo amplification of the androgen receptor gene and progression of human prostate cancer. *Nat. Genet.* **9**, 401–406 (1995).
32. Asangani, I. A. et al. Therapeutic targeting of BET bromodomain proteins in castration-resistant prostate cancer. *Nature* **510**, 278–282 (2014).
33. Roche, P. J., Hoare, S. A. & Parker, M. G. A consensus DNA-binding site for the androgen receptor. *Mol. Endocrinol.* **6**, 2229–2235 (1992).
34. Pomerantz, M. M. et al. The androgen receptor cistrome is extensively reprogrammed in human prostate tumorigenesis. *Nat. Genet.* **47**, 1346–1351 (2015).
35. Cancer Genome Atlas Research Network. The molecular taxonomy of primary prostate cancer. *Cell* **163**, 1011–1025 (2015).
36. Takayama, K. et al. Androgen-responsive long noncoding RNA CTBP1-AS promotes prostate cancer. *EMBO J.* **32**, 1665–1680 (2013).
37. GTEx Consortium. The Genotype-Tissue Expression (GTEx) pilot analysis: multitissue gene regulation in humans. *Science* **348**, 648–660 (2015).
38. Mele, M. et al. The human transcriptome across tissues and individuals. *Science* **348**, 660–665 (2015).
39. Rhodes, D. R. et al. OncoPrint 3.0: genes, pathways, and networks in a collection of 18,000 cancer gene expression profiles. *Neoplasia* **9**, 166–180 (2007).
40. Engreitz, J. M. et al. RNA-RNA interactions enable specific targeting of noncoding RNAs to nascent pre-mRNAs and chromatin sites. *Cell* **159**, 188–199 (2014).
41. Kretz, M. et al. Control of somatic tissue differentiation by the long non-coding RNA TINCR. *Nature* **493**, 231–235 (2013).
42. Gong, C. & Maquat, L. E. lncRNAs transactivate STAU1-mediated mRNA decay by duplexing with 3' UTRs via Alu elements. *Nature* **470**, 284–288 (2011).
43. Gawronski, A. R. et al. MechRNA: prediction of lncRNA mechanisms from RNA-RNA and RNA-protein interactions. *Bioinformatics* (2018) <https://doi.org/10.1093/bioinformatics/bty208>
44. Mann, M., Wright, P. R. & Backofen, R. IntaRNA 2.0: enhanced and customizable prediction of RNA-RNA interactions. *Nucleic Acids Res.* **45**, W435–W439 (2017).
45. Lennox, K. A. & Behlke, M. A. Cellular localization of long non-coding RNAs affects silencing by RNAi more than by antisense oligonucleotides. *Nucleic Acids Res.* **44**, 863–877 (2016).
46. Meng, L. et al. Towards a therapy for Angelman syndrome by targeting a long non-coding RNA. *Nature* **518**, 409–412 (2015).
47. Wheeler, T. M. et al. Targeting nuclear RNA for in vivo correction of myotonic dystrophy. *Nature* **488**, 111–115 (2012).
48. Hua, Y. et al. Antisense correction of SMN2 splicing in the CNS rescues necrosis in a type III SMA mouse model. *Genes Dev.* **24**, 1634–1644 (2010).
49. Evers, M. M., Toonen, L. J. & van Roon-Mom, W. M. Antisense oligonucleotides in the therapy for neurodegenerative disorders. *Adv. Drug Deliv. Rev.* **87**, 90–103 (2015).
50. Yeap, B. B. et al. Novel binding of HuR and poly(C)-binding protein to a conserved UC-rich motif within the 3'-untranslated region of the androgen receptor messenger RNA. *J. Biol. Chem.* **277**, 27183–27192 (2002).
51. Lebedeva, S. et al. Transcriptome-wide analysis of regulatory interactions of the RNA-binding protein HuR. *Mol. Cell* **43**, 340–352 (2011).

Acknowledgements

We thank A. Poliakov, A. Parolia, V. Kothari and J. Siddiqui for helpful discussions, the University of Michigan Sequencing Core for Sanger sequencing, H. Johansson (LGC-Biosearch) for initial assistance with smFISH probe design, and S. Ellison, S. Gao and K. Giles for critically reading the manuscript and submitting documents. This work was supported in part by NCI Prostate SPORE (P50CA186786 to A.M.C.) and EDNR (U01 CA214170 to A.M.C.) grants. A.M.C. is also supported by the Prostate Cancer Foundation and by the Howard Hughes Medical Institute. A.M.C. is an American Cancer Society Research Professor and a Taubman Scholar of the University of Michigan. R. Malik was supported by a Department of Defense Postdoctoral Award (W81XWH-13-1-0284). Y.Z. is supported by a Department of Defense Early Investigator Research Award (W81XWH-17-1-0134). R. Malik, M.C., Y.S.N., J.C.-Y.T. and Y.Q. were supported by the Prostate Cancer Foundation Young Investigator Award. R. Mehra was supported by a Department of Defense Idea Development Award (W81XWH-16-1-0314). Y.S.N. is supported by a University of Michigan Cellular and Molecular Biology National Research Service Award Institutional Predoctoral Training Grant. S.P. was supported by an AACR-Bayer Prostate Cancer Research Fellowship (16-40-44-PITC). L.X. is supported by a US Department of Defense Postdoctoral Fellowship (W81XWH-16-1-0195). M.B. was supported by NIH DP5 grant OD012160. G.C.S. was supported by the Department of Defense awards W81XWH-14-1-0508 and

W81XWH-14-1-0509. M.U. was funded by the German Research Foundation (DFG grant BA2168/11-1 SPP 1738).

Author contributions

R. Malik, Y.Z., M.C., S.P. and A.M.C. conceived the study and designed the research. Y.Z. and R. Malik performed most of the cellular and molecular biology experiments with the assistance of Y.H., S.Y., S.S., S.K.S., L.X., X.J., S.M.D., X.C., J.T.W. and F.Y.F. M.C. performed most of the bioinformatics analyses with the help of Y.S.N. and M.K.I. S.P., U.P. and M.B. performed all smFISH work, and S.P. performed the mechanistic work-up. J.C.-Y.T. and K.M.J. carried out the *in vivo* mouse xenograft studies, and Y.Q. performed the 3D sphere model work. L.P.K. performed the histopathological analyses. L.W. and R. Mehra carried out RNA ISH on tissue microarrays, and T.-Y.L. and H.J. performed the statistical analysis for this technique. M.U., A.R.G., R.B. and C.S.S. performed the *in silico* binding predictions. S.M.F., A.T.W. and S.G. provided ASOs. G.C.S. provided the AR expression construct. M.T.P. and M.L. performed BrU and BrUChase sample preparation. Y.Z., M.C., R. Malik, S.P. and A.M.C. wrote the manuscript. All authors discussed the results and commented on the manuscript.

Competing interests

The University of Michigan has filed a patent on lncRNAs as biomarkers of cancer, and A.M.C., R. Malik, Y.Z., M.C. and S.P. are named as co-inventors. A.M.C. is a co-founder of LynxDx, which is developing lncRNA biomarkers. S.M.F., A.T.W. and S.G. are employees of Ionis Pharmaceuticals, which developed the ASOs against *ARLNC1* that were used in this study.

Additional information

Supplementary information is available for this paper at <https://doi.org/10.1038/s41588-018-0120-1>.

Reprints and permissions information is available at www.nature.com/reprints.

Correspondence and requests for materials should be addressed to A.M.C.

Publisher's note: Springer Nature remains neutral with regard to jurisdictional claims in published maps and institutional affiliations.

Methods

Cell lines. Cell lines were purchased from the American Type Culture Collection (ATCC) and maintained using standard media and conditions. All cell lines were genotyped by DNA fingerprinting analysis and tested for mycoplasma infection every 2 weeks. All cell lines used in this study were mycoplasma negative. For androgen stimulation experiments, VCaP and LNCaP cells were grown in medium supplemented with charcoal-stripped serum for 48 h and then stimulated with 10 nM DHT (Sigma-Aldrich) for 6 or 24 h.

RNA-seq. Total RNA was extracted from LNCaP and VCaP cells following DHT treatment, using the miRNeasy kit (Qiagen). RNA quality was assessed using an Agilent Bioanalyzer. Each sample was sequenced using the Illumina HiSeq 2000 (with a 100-nt read length) according to published protocols⁵².

RNA-seq data analysis to identify AR-regulated genes. RNA-seq data were analyzed as previously described⁵³. Briefly, the strand-specific paired-end reads were inspected for sequencing and data quality (for example, insert size, sequencing adaptor contamination, rRNA content, sequencing error rate). Libraries passing quality control were trimmed of sequencing adaptors and aligned to the human reference genome, GRCh38. Expression was quantified at the gene level using the 'intersection non-empty' mode⁵⁴ as implemented in featureCounts⁵⁵ using the Gencode v22⁵⁶ and/or MiTranscriptome¹⁰ assemblies. All pairwise differential expression analyses were carried out using the voom-limma approach^{57,58} with all default parameters. Relative expression levels (FPKM) were normalized for differences in sequencing depth using scaling factors obtained from the calcNormFactors (default parameters) function from edgeR⁵⁹.

ARGs were identified from expression data for VCaP and LNCaP cells treated with DHT for 6 and 24 h using three linear models: separate models for each of the cell lines treating the two time points as biological replicates and a merged model with all treated samples as replicates. ARGs were defined as genes that were significant (P value < 0.1 and absolute log fold change > 2) in both separate models and/or the merged model.

Identification of prostate cancer-associated protein-coding genes and lncRNAs.

Raw RNA-seq data for patients with primary and metastatic prostate cancer were obtained from the TCGA/PRAD and PCF/SU2C projects, respectively. External transcriptome samples were reanalyzed using in-house pipelines (see above) to facilitate direct comparisons of expression levels and identification of differentially expressed genes. Pan-cancer analyses based on the MiTranscriptome assembly¹⁰ were leveraged as FPKMs, and enrichment scores (SSEA) were computed as part of that project. Tissue lineage (prostate) and prostate cancer-specific genes were identified using the SSEA method as previously described¹⁰. Briefly, the SSEA test was used to determine whether each gene was significantly associated with a set of samples (for example, prostate cancer) or cancer progression in a given lineage (for example, prostate normal to prostate cancer). The genes were ranked according to their strength of association.

Oncomine concept analysis of the ARLNC1 signature. Genes with expression levels significantly correlated with ARLNC1 were separated into positively and negatively correlated gene lists. These two lists were then imported into Oncomine as custom concepts and queried for association with other prostate cancer concepts housed in Oncomine. All of the prostate cancer concepts with odds ratio > 2.0 and P value $< 1 \times 10^{-4}$ were selected. Top concepts (based on odds ratios) were selected for representation. We exported these results as the nodes and edges of a concept association network and visualized the network using Cytoscape version 3.3.0. Node positions were computed using the edge-weighted force-directed layout in Cytoscape using the odds ratio as the edge weight. Node positions were subtly altered manually to enable better visualization of Mode labels⁶⁰.

ChIP-seq data analysis. ChIP-seq data from published external and in-house datasets, GSE56288 and GSE55064, were reanalyzed using a standard pipeline. Briefly, groomed reads (vendor quality control, adaptor removal) were aligned to the GRCh38 reference genome using STAR settings that disable spliced alignment: outFilterMismatchNoverLmax: 0.05, outFilterMatchNmin: 16, outFilterScoreMinOverLread: 0, outFilterMatchNminOverLread: 0, alignIntronMax: 1. Improperly paired alignments and non-primary alignments were discarded. Peaks were called using MACS2 (callpeak --broad --qvalue 0.05 --broad-cutoff 0.05 and callpeak --call-summits --qvalue 0.05)⁶¹ and Q (-n 100000)⁶². ChIP enrichment plots were computed from alignment coverage files (BigWig⁶³) as trimmed (trim = 0.05) smooth splines (spar = 0.05). The baseline (non-specific) ChIP signal was estimated from genomic windows furthest from the center of the queried region (peak summit, TSS) and subtracted from each signal before plotting.

AR binding motif search. An unsupervised motif search was carried out using MEME⁶⁴. DNA sequences (GRCh38) from the uni-peak ChIP-seq regions overlapping promoters (5 kb upstream, 1 kb downstream of the assembled or known TSS) of ARGs were used as input to MEME (default parameters).

ChIP-qPCR assays. AR, FOXA1 or NKX3-1 ChIP was performed following our previous protocol⁵². (Antibodies: AR, Millipore cat. no. 06-680; FOXA1, Thermo Fisher cat. no. PA5-27157; NKX3-1, CST cat. no. 837005.) qPCR analysis was performed using the primers listed in Supplementary Table 3. Primers targeting the *CYP2B7* promoter were purchased from CST (cat. no. 84846).

RNA ISH on tissue microarray. ISH assays were performed on tissue microarray sections from Advanced Cell Diagnostics as described previously⁷. In total, 133 tissue samples were included (11 from benign prostate, 85 from localized prostate cancer and 37 from metastatic prostate cancer). ARLNC1 ISH signals were examined in morphologically intact cells and scored manually by a study pathologist, using a previously described expression value scoring system⁶⁵. For each tissue sample, the ARLNC1 product score was averaged across evaluable tissue microarray cores. Mean ARLNC1 product scores are plotted in Fig. 2e.

RACE. 5' and 3' RACE were performed to determine the transcriptional start and termination sites of ARLNC1, using the GeneRacer RLM-RACE kit (Invitrogen), according to the manufacturer's instructions.

Northern blot analysis. The NorthernMax-Gly Kit (Ambion) was used for ARLNC1 detection following the manufacturer's protocol. Briefly, 20 μ g of total RNA was resolved on a 1% agarose glyoxal gel and then transferred to nylon membrane (Roche), cross-linked to the membrane (UV Stratalinker 1800; Stratagene) and the membrane was prehybridized. Overnight hybridization was performed with an ARLNC1-specific ³²P-labeled RNA probe. Membranes were exposed to HyBlot CL autoradiography film (Denville Scientific). The primer sequences used for generating the probes are given in Supplementary Table 3.

RNA isolation and cDNA synthesis. Total RNA from cell lines was isolated using QIAzol Lysis reagent (Qiagen) and the miRNeasy kit (Qiagen) with DNase digestion according to the manufacturer's instructions. cDNA was synthesized using Superscript III (Invitrogen) and random primers (Invitrogen).

qRT-PCR analysis. Relative RNA levels determined by qRT-PCR were measured on an Applied Biosystems 7900HT Real-Time PCR System, using Power SYBR Green MasterMix (Applied Biosystems). All primers were obtained from Integrated DNA Technologies, and gene-specific sequences are listed in Supplementary Table 3. *GAPDH*, *HMBS* or *ACTB* was used as an internal control for quantification of gene targets. The relative expression of RNAs was calculated using the $\Delta\Delta Ct$ method.

Cytoplasmic and nuclear RNA purification. Cell fractionation was performed using the NE-PER nuclear extraction kit (Thermo Scientific) according to the manufacturer's instructions. RNA was extracted using the previously mentioned protocol.

siRNA-mediated knockdown. siRNA oligonucleotides targeting ARLNC1, AR, FOXA1, BRD4, NKX3-1, LSD1, IRF1, POU1F1 or EZH2 and a non-targeting siRNA were purchased from Dharmacon. (si-AR-pool, cat. no. L-003400-00-0005; si-FOXA1, cat. no. LU-010319-00-0005; si-BRD4, cat. no. LU-004937-00-0002; si-NKX3-1, cat. no. LU-015422-00-0005; si-LSD1, cat. no. LU-009223-00-0002; si-IRF1, cat. no. LU-011704-00-0005; si-POU1F1, cat. no. LU-012546-00-0005; si-EZH2, cat. no. L-004218-00-0005; si-NT, cat. no. D-001810-01-05.) siRNA sequences for ARLNC1 knockdown are listed in Supplementary Table 3. For AR knockdown, two more siRNAs were purchased from Life Technologies (no. HSS179972 and no. HSS179973). Transfections with siRNA (50 nM) were performed with Lipofectamine RNAiMAX according to the manufacturer's instructions. RNA and protein were harvested for analysis 72 h after transfection.

ASO-mediated knockdown. ASOs targeting ARLNC1 were obtained from Ionis Pharmaceuticals. Transfections with ASOs (50 nM) were performed with Lipofectamine RNAiMAX according to the manufacturer's instructions. RNA and protein were harvested for analysis 72 h after transfection.

Gene expression profiling. Total RNA was extracted following the aforementioned protocol. RNA integrity was assessed using an Agilent Bioanalyzer. Microarray analysis was carried out on the Agilent Whole Human Oligo Microarray platform, according to the manufacturer's protocol. siRNA-mediated knockdown experiments were run in triplicate, comparing knockdown samples treated with two independent ARLNC1 siRNAs to samples treated with non-targeting control siRNA. ASO-mediated knockdown experiments were run in replicate, comparing knockdown samples treated with two ARLNC1 ASOs to samples treated with non-targeting control. An AR signature was generated using MDA-PCA-2b cells treated with 10 nM DHT in triplicate.

Analysis of Agilent 44k microarrays was carried out using limma and included background subtraction (bc.method = 'half', offset = 100) and within-array normalization (method = 'loess'). Between-array quantile normalization of average expression levels (but not log-transformed fold change) was performed using the function normalizeBetweenArrays (method = 'Aquantile'). Control probes and

probes with missing values were excluded from further analyses. Probes were annotated to Gencode v22 genes using the mapping downloaded from Ensembl (efg_agilent_wholegenome_4x44k_v2). Probes originally annotated as AK093002 were used to detect *ARLNC1*. Differentially expressed genes following *ARLNC1* knockdown in MDA-PCA-2b cells were identified from triplicate biological repeats using adjusted *P* value < 0.1 and absolute log fold change > 0.6 cutoffs. Consensus targets of *ARLNC1* knockdown using siRNA and ASOs were identified using a merged linear model (all ten samples treated as replicates) and a *P* value < 0.001 cutoff.

GSEA. Enrichment analyses for custom and experimentally derived signatures (that is, AR targets, genes upregulated and downregulated following DHT treatment) were carried out using the non-parametric GSEA software with all default settings. For GO term enrichment, we applied the parametric randomSet⁶⁶ enrichment statistic to voom–limma-estimated fold changes (see above).

Overexpression of *ARLNC1*. Full-length *ARLNC1* was amplified from MDA-PCA-2b cells and cloned into the pCDH clone and expression vector (System Biosciences). Insert sequences were validated by Sanger sequencing at the University of Michigan Sequencing Core. The full-length sequence for *ARLNC1* expression is listed in Supplementary Table 4.

smFISH. smFISH and image analysis were performed as described previously^{67,68}. Probe sequences targeting *ARLNC1*, *PCAT1*, *DANCR*, *AR*, *EZH2* and *FOXA1* were designed using the probe design software at <https://www.biosearchtech.com/stellaris-designer> and are listed in Supplementary Table 5. TERRA probes were designed as described previously⁶⁹. Other probes were purchased directly from LGC-Biosearch. U2OS cells were seeded in six-well dishes and transfected with *ARLNC1*-expression vector alone or in combination with AR expression vector, using Fugene-HD (Promega) according to the manufacturer's protocol. Cells were incubated for 24 h, reseeded into eight-well chambered coverglasses, and fixed in formaldehyde for smFISH (as described above) after 24 h.

RNA in vitro transcription. Linearized DNA templates for full-length *ARLNC1*, *ARLNC1* fragments, *ARLNC1* deletion, antisense *ARLNC1*, *LacZ*, *SChLAP1-AS*, *THOR* and *AR-3' UTR-1-980* were synthesized using T7-containing primers. In vitro transcription assays were performed with T7 RNA polymerase (Promega) according to the manufacturer's instructions. For BrU-labeled RNA synthesis, 5-bromo-UTP was added to the transcription mix. At the end of transcription, DNA templates were removed by Turbo DNase (Thermo Fisher), and RNA was recovered using the RNA Clean and Concentrator Kit (Promega). RNA size and quality were further confirmed by Agilent Bioanalyzer.

RNA–RNA in vitro interaction assays. Twenty-five microlitres of Protein A/G Magnetic Beads (Pierce) was washed twice with RIP wash buffer (Millipore, cat. no. CS203177) before incubating with BrU antibody for 1 h at room temperature. After antibody conjugation, beads were washed twice with RIP wash buffer and then resuspended in incubation buffer containing RIP wash buffer, 17.5 mM EDTA (Millipore, cat. no. CS203175) and RNase Inhibitor (Millipore, cat. no. CS203219). Equal amounts (5 pmol) of BrU-labeled RNAs (*ARLNC1*, *ARLNC1-AS*, *ARLNC1-1-1300*, *ARLNC1-1301-2786*, *ARLNC1-1-700*, *ARLNC1-701-1300*, *ARLNC1-del-701-1300*, *LacZ*, *SChLAP1-AS*, *THOR*) were incubated with beads in Incubation Buffer for 2 h at 4 °C. Following incubation, 2.5 pmol of the *AR 3' UTR-1-980* RNA fragment was added into individual tubes and incubated overnight at 4 °C. After incubation, beads were washed six times with RIP Wash Buffer. To recover RNA, beads were digested with proteinase K buffer containing RIP Wash Buffer, 1% SDS (Millipore, cat. no. CS203174) and 1.2 μg/μl proteinase K (Millipore, cat. no. CS203218) at 55 °C for 30 min with shaking. After digestion, RNA was extracted from supernatant using the miRNeasy kit (Qiagen), and reverse transcription was performed using the Superscript III system (Invitrogen). The amount of *AR 3' UTR-1-980* recovered in each interaction assay was quantified by qPCR analysis. Data were normalized to the *ARLNC1-AS* control, using the ΔCt method. We designed ASOs blocking the *AR-ARLNC1* interaction site (ASO-blocking, Ionis Pharmaceuticals) and used them in the in vitro interaction assays. Data were normalized to the control ASO, using the ΔCt method.

RNA stability assays. LNCaP cells were treated with 5 μg/ml actinomycin D for various times as indicated. RNA was extracted and qRT-PCR was carried out as described above. RNA half-life ($t_{1/2}$) was calculated by linear regression analysis.

Cell proliferation assays. Cells treated with siRNAs or ASOs were seeded into 24-well plates and allowed to attach. Cell proliferation was recorded by IncuCyte live-cell imaging system (Essen Biosciences), following the manufacturer's instructions.

Apoptosis analysis. Cells were grown in six-well plates and transfected with nonspecific siRNA or siRNAs targeting *ARLNC1*. Apoptosis analysis was performed 48 h after transfection, using the Dead Cell Apoptosis Kit (Molecular Probes no. V13241) according to the manufacturer's instructions.

Immunoblot analysis. Cells were lysed in RIPA lysis and extraction buffer (Thermo Scientific no. 89900) supplemented with protease inhibitor cocktail (Roche no. 11836170001). Protein concentrations were quantified using the DC protein assay (Bio-Rad), and protein lysates were boiled in sample buffer. Protein extracts were then loaded and separated on SDS–PAGE gels. Blotting analysis was performed with standard protocols using polyvinylidene difluoride membrane (GE Healthcare). Membranes were blocked for 60 min in blocking buffer (5% milk in a solution of 0.1% Tween-20 in Tris-buffered saline (TBS-T)) and then incubated overnight at 4 °C with primary antibody. After three washes with TBS-T, membranes were incubated with horseradish peroxidase (HRP)-conjugated secondary antibody. Signals were visualized with an enhanced chemiluminescence system as described by the manufacturer (Thermo Scientific Pierce ECL Western Blotting Substrate). Primary antibodies used were as follows: androgen receptor (1:1,000 dilution, Millipore, no. 06-680, rabbit), GAPDH (1:5,000 dilution, Cell Signaling, no. 3683, rabbit), PSA (KLK3) (1:5,000 dilution, Dako, no. A0562, rabbit) and cleaved PARP (1:1,000 dilution, Cell Signaling, no. 9542, rabbit).

Androgen receptor reporter gene assays. Dual-luciferase reporter assays were performed using the Cignal Androgen Receptor Reporter Kit (Qiagen) according to the manufacturer's instructions. Briefly, cells were cotransfected with siRNAs (nonspecific, targeting *AR* or *ARLNC1*) and reporter vectors (negative control or AR reporter), using Lipofectamine 2000 transfection reagent (Thermo Fisher Scientific). Forty hours after transfection, DHT (or ethanol vehicle control) was added to induce AR signaling. The Dual-Luciferase assay was conducted 8 h after DHT stimulation, using the Dual-Luciferase Reporter Assay System from Promega (cat no. 1910). Reporter activity was analyzed on the basis of the ratio of firefly/*Renilla* activity to normalize for cell number and transfection efficiency.

In vivo experiments. All experiments were approved by the University of Michigan Institutional Animal Care and Use Committee. For tumor generation with shRNA-mediated knockdown, shRNA targeting *ARLNC1* was cloned into pSIH1-H1-copGFP-T2A-Puro (System Biosciences). Lentiviral particles were generated at the University of Michigan Vector Core. LNCaP-AR cells were infected with lentivirus expressing *ARLNC1* shRNA for 48 h. Knockdown of *ARLNC1* was confirmed by qPCR analysis. Male athymic nude mice were randomized into two groups at 6 to 8 weeks of age. Five million cells expressing sh-*ARLNC1* or sh-vector were injected into bilateral flanks of mice. Caliper measurements were taken in two dimensions twice a week by an investigator blinded to the study objective and used to calculate tumor volume. The study was terminated when the tumor volume reached 1,000 mm³. For ASO treatment in vivo, 6- to 8-week-old male athymic nude mice were inoculated subcutaneously with MDA-PCA-2b cells suspended in a Matrigel scaffold in the posterior dorsal flank region (5 million cells per site, two sites per animal). When the mean tumor volume reached approximately 150 mm³, mice were randomized into two groups and treated with *ARLNC1*-specific or control ASO. ASOs, dosed at 50 mg per kg body weight, were subcutaneously injected between the scapulae once daily for three periods of 5 d on/2 d off. Tumor size was measured twice per week using a digital caliper by a researcher blinded to the study design. Mouse body weights were monitored throughout the dosing period. When the average tumor size in the control group reached 1,500 mm³, mice were euthanized and the primary tumors were excised for weight determination. One-third of the resected specimen was placed in 10% formalin buffer, and the remaining tissue was snap-frozen.

BrU-seq and BrUChase-seq. BrU-seq and BrUChase-seq assays were performed as previously described^{70,71} with MDA-PCA-2b cells treated with either si-NT or si-*ARLNC1*. BrU labeling was performed for 30 min, and chase experiments were performed for 6 h.

Statistical analysis. For in vivo experiments, power analysis (GPOWER software) performed for each tumor type tested to date indicates that the sample size we chose yields a statistical power >90% for detection of tumor size reduction of 40%. Sample sizes were not predetermined for all other assays. For in vivo experiments, animals were randomized. Randomization was not performed for all other assays. Statistical analyses were performed using GraphPad Prism software or using R. Data are presented as either means ± s.e.m. or means ± s.d. All of the experiments were performed in biological triplicate unless otherwise specified. Statistical analyses shown in figures represent two-tailed *t* tests, one-way ANOVA, two-way ANOVA or Kruskal–Wallis rank-sum tests as indicated. *P* < 0.05 was considered to be statistically significant. Details regarding the statistical methods employed during microarray, RNA-seq and ChIP-seq data analysis were included in the aforementioned methods for bioinformatics analyses.

Reporting Summary. Further information on experimental design is available in the Nature Research Reporting Summary linked to this article.

Code availability. Software for transcriptome meta-assembly and lncRNA discovery is available at <https://tacorna.github.io/>.

Data availability. RNA-seq and microarray data sets generated from this study have been deposited into the Gene Expression Omnibus, with accession [GSE110905](https://www.ncbi.nlm.nih.gov/geo/query/acc.cgi?acc=GSE110905). Other data supporting the findings of this study are included in the Supplementary Information.

References

52. Prensner, J. R. et al. Transcriptome sequencing across a prostate cancer cohort identifies PCAT-1, an unannotated lincRNA implicated in disease progression. *Nat. Biotechnol.* **29**, 742–749 (2011).
53. Cieslik, M. et al. The use of exome capture RNA-seq for highly degraded RNA with application to clinical cancer sequencing. *Genome Res.* **25**, 1372–1381 (2015).
54. Anders, S., Pyl, P. T. & Huber, W. HTSeq—a Python framework to work with high-throughput sequencing data. *Bioinformatics* **31**, 166–169 (2015).
55. Liao, Y., Smyth, G. K. & Shi, W. featureCounts: an efficient general purpose program for assigning sequence reads to genomic features. *Bioinformatics* **30**, 923–930 (2014).
56. Harrow, J. et al. GENCODE: the reference human genome annotation for The ENCODE Project. *Genome Res.* **22**, 1760–1774 (2012).
57. Law, C. W., Chen, Y., Shi, W. & Smyth, G. K. voom: precision weights unlock linear model analysis tools for RNA-seq read counts. *Genome Biol.* **15**, R29 (2014).
58. Ritchie, M. E. et al. limma powers differential expression analyses for RNA-sequencing and microarray studies. *Nucleic Acids Res.* **43**, e47 (2015).
59. Robinson, M. D., McCarthy, D. J. & Smyth, G. K. edgeR: a Bioconductor package for differential expression analysis of digital gene expression data. *Bioinformatics* **26**, 139–140 (2010).
60. Cline, M. S. et al. Integration of biological networks and gene expression data using Cytoscape. *Nat. Protoc.* **2**, 2366–2382 (2007).
61. Zhang, Y. et al. Model-based analysis of ChIP-Seq (MACS). *Genome Biol.* **9**, R137 (2008).
62. Hansen, P. et al. Saturation analysis of ChIP-seq data for reproducible identification of binding peaks. *Genome Res.* **25**, 1391–1400 (2015).
63. Kent, W. J., Zweig, A. S., Barber, G., Hinrichs, A. S. & Karolchik, D. BigWig and BigBed: enabling browsing of large distributed datasets. *Bioinformatics* **26**, 2204–2207 (2010).
64. Bailey, T. L. et al. MEME SUITE: tools for motif discovery and searching. *Nucleic Acids Res.* **37**, W202–W208 (2009).
65. Mehra, R. et al. A novel RNA in situ hybridization assay for the long noncoding RNA SCHLAP1 predicts poor clinical outcome after radical prostatectomy in clinically localized prostate cancer. *Neoplasia* **16**, 1121–1127 (2014).
66. Newton, M. A., Quintana, F. A., Den Boon, J. A., Sengupta, S. & Ahlquist, P. Random-set methods identify distinct aspects of the enrichment signal in gene-set analysis. *Ann. Appl. Stat.* **1**, 85–106 (2007).
67. Raj, A., van den Bogaard, P., Rifkin, S. A., van Oudenaarden, A. & Tyagi, S. Imaging individual mRNA molecules using multiple singly labeled probes. *Nat. Methods* **5**, 877–879 (2008).
68. Niknafs, Y. S. et al. The lincRNA landscape of breast cancer reveals a role for DSCAM-AS1 in breast cancer progression. *Nat. Commun.* **7**, 12791 (2016).
69. Rossiello, F. et al. DNA damage response inhibition at dysfunctional telomeres by modulation of telomeric DNA damage response RNAs. *Nat. Commun.* **8**, 13980 (2017).
70. Paulsen, M. T. et al. Coordinated regulation of synthesis and stability of RNA during the acute TNF-induced proinflammatory response. *Proc. Natl Acad. Sci. USA* **110**, 2240–2245 (2013).
71. Paulsen, M. T. et al. Use of Bru-Seq and BruChase-Seq for genome-wide assessment of the synthesis and stability of RNA. *Methods* **67**, 45–54 (2014).

Reporting Summary

Nature Research wishes to improve the reproducibility of the work that we publish. This form provides structure for consistency and transparency in reporting. For further information on Nature Research policies, see [Authors & Referees](#) and the [Editorial Policy Checklist](#).

Statistical parameters

When statistical analyses are reported, confirm that the following items are present in the relevant location (e.g. figure legend, table legend, main text, or Methods section).

n/a Confirmed

- The exact sample size (n) for each experimental group/condition, given as a discrete number and unit of measurement
- An indication of whether measurements were taken from distinct samples or whether the same sample was measured repeatedly
- The statistical test(s) used AND whether they are one- or two-sided
Only common tests should be described solely by name; describe more complex techniques in the Methods section.
- A description of all covariates tested
- A description of any assumptions or corrections, such as tests of normality and adjustment for multiple comparisons
- A full description of the statistics including central tendency (e.g. means) or other basic estimates (e.g. regression coefficient) AND variation (e.g. standard deviation) or associated estimates of uncertainty (e.g. confidence intervals)
- For null hypothesis testing, the test statistic (e.g. F , t , r) with confidence intervals, effect sizes, degrees of freedom and P value noted
Give P values as exact values whenever suitable.
- For Bayesian analysis, information on the choice of priors and Markov chain Monte Carlo settings
- For hierarchical and complex designs, identification of the appropriate level for tests and full reporting of outcomes
- Estimates of effect sizes (e.g. Cohen's d , Pearson's r), indicating how they were calculated
- Clearly defined error bars
State explicitly what error bars represent (e.g. SD, SE, CI)

Our web collection on [statistics for biologists](#) may be useful.

Software and code

Policy information about [availability of computer code](#)

Data collection

RNA seq, Microarray and qRT-PCR data were collected using vendor's software on Illumina HiSeq 2000, Agilent Whole Human Oligo Microarray, Applied Biosystems 7900HT Real-Time PCR platforms respectively. Microscopy images were acquired using Metamorph.

Data analysis

Software for transcriptome meta-assembly and lncRNAs discovery is available at <https://tacorna.github.io/>. Gene signatures were obtained using GSEA software. Image analysis was performed using custom-written macros in Image J and can be shared upon request. Statistical analysis was performed using Graphpad-Prism 6.0 and R.

For manuscripts utilizing custom algorithms or software that are central to the research but not yet described in published literature, software must be made available to editors/reviewers upon request. We strongly encourage code deposition in a community repository (e.g. GitHub). See the Nature Research [guidelines for submitting code & software](#) for further information.

Data

Policy information about [availability of data](#)

All manuscripts must include a [data availability statement](#). This statement should provide the following information, where applicable:

- Accession codes, unique identifiers, or web links for publicly available datasets
- A list of figures that have associated raw data
- A description of any restrictions on data availability

RNA-seq and microarray datasets generated from this study have been deposited into Gene Expression Omnibus, with accession number: GSE110905. Other data supporting the finding of this study are included in the Supplementary Information files. Software for transcriptome meta-assembly and lncRNAs discovery is available at <https://tacorna.github.io/>. We have no restrictions on data availability and data can be shared upon request.

Field-specific reporting

Please select the best fit for your research. If you are not sure, read the appropriate sections before making your selection.

Life sciences Behavioural & social sciences

For a reference copy of the document with all sections, see nature.com/authors/policies/ReportingSummary-flat.pdf

Life sciences

Study design

All studies must disclose on these points even when the disclosure is negative.

Sample size	For in vivo experiments, power analysis (GPOWER software) performed for each tumor type tested to date indicates this animal number yields a statistical power >90% for detection of tumor size reduction of 40%. Sample sizes were not pre-determined for all other assays.
Data exclusions	No data were excluded.
Replication	All experiments were carried out at least 3 independent times for statistical reproducibility, unless otherwise stated, as represented by p-values.
Randomization	For in vivo experiments, animals were randomized. Randomization was not performed for all other assays.
Blinding	For in vivo experiments, tumor size was measured twice per week using a digital caliper by a researcher blinded to the study design. Blinding was not performed for all other assays.

Materials & experimental systems

Policy information about [availability of materials](#)

n/a	Involved in the study
<input checked="" type="checkbox"/>	<input type="checkbox"/> Unique materials
<input type="checkbox"/>	<input checked="" type="checkbox"/> Antibodies
<input type="checkbox"/>	<input checked="" type="checkbox"/> Eukaryotic cell lines
<input type="checkbox"/>	<input checked="" type="checkbox"/> Research animals
<input checked="" type="checkbox"/>	<input type="checkbox"/> Human research participants

Antibodies

Antibodies used	Primary antibodies used in this study were: Androgen Receptor (1:1000 dilution, Millipore, #06-680, rabbit), GAPDH (1:5000 dilution, Cell Signaling, #3683, rabbit), PSA (1:5000 dilution, Dako, #A0562, rabbit), FOXA1 (Thermo Fisher Cat# PA5-27157) NKX3.1 (CST Cat# 837005) and cleaved PARP (1:1000 dilution, Cell Signaling, #9542, rabbit).
Validation	All antibodies were validated by the vendors. Androgen receptor and PSA antibodies were also validated by siRNA treatment and androgen signaling assays respectively.

Eukaryotic cell lines

Policy information about [cell lines](#)

Cell line source(s)	All cell lines were purchased from ATCC.
Authentication	All cell lines were genotyped by STR profiling in house based on ATCC markers.

Mycoplasma contamination

All cells were tested for mycoplasma every two weeks.

Commonly misidentified lines
(See [ICLAC](#) register)

Study does not include misidentified lines.

Research animals

Policy information about [studies involving animals](#); [ARRIVE guidelines](#) recommended for reporting animal research

Animals/animal-derived materials

Male athymic nude mice were used in our in vivo studies.

Method-specific reporting

n/a	Involvement in the study
<input checked="" type="checkbox"/>	<input type="checkbox"/> ChIP-seq
<input checked="" type="checkbox"/>	<input type="checkbox"/> Flow cytometry
<input checked="" type="checkbox"/>	<input type="checkbox"/> Magnetic resonance imaging